DEVELOPMENT OF A MULTICOLOR AUTONOMOUS BIOLUMINESCENCE IMAGING TECHNOLOGY

BY

SUBHAN HADI KUSUMA

AUGUST 2024

A THESIS SUBMITTED TO
GRADUATE SCHOOL OF FRONTIER BIOSCIENCES
OSAKA UNIVERSITY FOR
THE DEGREE OF
DOCTOR OF PHILOSOPHY
ACADEMIC YEAR 2024

ABSTRACT

Bioluminescence imaging has become a valuable tool in biological research, offering several advantages over fluorescence-based techniques, including the absence of phototoxicity and photobleaching, as well as a higher signal-to-noise ratio. Common bioluminescence imaging methods often require the addition of an external chemical substrate (luciferin), which can result in a decrease in luminescence intensity over time and limit prolonged observation. Because the bacterial bioluminescence system is genetically encoded for luciferase-luciferin production, it enables autonomous bioluminescence (auto-bioluminescence) imaging. However, its application to multiple reporters is restricted because of the limited range of color variants. In this thesis, I present a novel multicolor auto-bioluminescence system named Nano-lanternX (NLX), derived from **N**ano-lantern based on Lu**x**. NLXs were developed by bioluminescence resonance energy transfer (BRET) from Lux as the donor and specific fluorescent proteins, such as mTurquoise2, sfGFP, Venus, mKOκ, and mScarlet-I, as the acceptor to generate cyan, green, yellow, orange, and red color variants, respectively. NLXs not only shifted the emission wavelength of Lux, but also increased the luminescence intensity by up to ten-fold owing to the enhancement of the luminescent quantum yield. I successfully applied NLXs to express in bacterial, mammalian and plant hosts, thereby, enabling multiplexed auto-bioluminescence imaging in various living organisms. In addition, I expanded the application of NLXs, not only with a single reporter, but also with multiplex gene reporter assays and protein localization. For the first time, using the strategy of changing the wavelength of Lux, I successfully engineered a Ca^{2+} and ATP sensor for auto-bioluminescence technology. Overall, NLXs are promising auto-bioluminescence technologies for future investigations of biological phenomena.

TABLE OF CONTENTS

LIST OF ABBREVIATIONS

Symbols/Abbreviations	Terms
ATP	Adenosine triphosphate
BNAH	Biomimetic nicotinamide
BP	Bioluminescence protein
BRET	Bioluminescence resonance energy transfer
Ca^{2+}	Calcium ion
CT	Threshold cycles
CCD	Charge-coupled device
cpVenus	Circularly permutated Venus
DMEM	Dulbecco's modified Eagle's medium
EM-CCD	Electron Multiplying CCD
eNL	Enhanced Nano-lantern
FMN	Flavin mononucleotide
$FMNH_2$	Reduced flavin mononucleotide
FP	Fluorescent protein
FRET	Förster resonance energy transfer
FRP	Flavin reductase protein
FLuc	Firefly luciferase
GFP	Green fluorescent protein
HTS	High-throughput screening
k_{cat}	Catalytic constant

K_d	Dissociation constant
K_m	Michaelis constant
KZK	Kozak
LiCl	Lithium chloride
mTQ2	mTurquoise2
mKOκ	mKusabira-Orange κ
NADPH	Nicotinamide adenine dinucleotide phosphate
NL	Nano-lantern
NLX	Nano-lantern based on Lux
NLuc	Nano-Luc luciferase
PBS	Phosphate buffered saline solutions
PDB	Protein Data Bank
QY	Quantum yield
RET	Resonance energy transfer
RLuc	Renilla luciferase
RLU	Relative luminescence intensity
SD	Standard deviation
sfGFP	Superfolder green fluorescent protein
TCF/LEF	T-cell factor/lymphoid enhancer-binding factor
TIM	Triose-phosphate isomerase
TEDA	T5 exonuclease-dependent assembly
V_{max}	Maximal velocity

CHAPTER 1

GENERAL INTRODUCTION

1.1 Bioluminescence

Bioluminescence is the transformation of chemical energy into light by living cells, a process that is facilitated by enzymes called luciferases and their specific substrates, luciferin. Luciferase catalyzes the transformation of luciferin into an electronically excited product, which, upon returning to its ground state, emits a photon, resulting in the production of bioluminescence light[1].

The use of luciferase and its corresponding luciferin has been primarily observed in living organisms that produce them. Several luciferases are frequently used in bioscience applications (**Table 1**). Firefly luciferase, also known as FLuc, is commonly used in research and is derived from the firefly species, *Photinus pyralis*. FLuc is an ATP-dependent luciferase, which requires both luciferin and ATP to produce light[2]. However, researchers have also discovered and engineered ATP-independent luciferases that do not require ATP for light emission. These ATP-independent luciferases have become increasingly popular among researchers. NanoLuc (NLuc) is the brightest ATP-independent luciferase currently available and is derived from the deep-sea shrimp, *Oplophorus gracilirostris*[3]. It converts furimazine, a luciferin, into furimamide, and emits bioluminescent light. This luciferase is smaller than other common ones, with a molecular weight of only 19 kDa. While NanoLuc, like other luciferases, needs luciferin to be added exogenously for use in bioscience applications, this approach can lead to increased autoxidation of luciferin and limitations on the prolonged observation of biological phenomena.

Consequently, genetically encoded luciferase-luciferin systems are preferred as optimal probes for bioluminescence imaging of living organisms.

Table 1. List of common luciferases for bioscience application

Luciferase	Organisms	Substrate	Cofactor(s)	Size (kDa)	Emission peak (nm)
Firefly (FLuc)	*Photinus pyralis*	D-luciferin	ATP and Mg	61	560
Click beetle	*Pyrophorus plagiophthalamus*	D-luciferin	ATP and Mg	64	~600
Renilla (RLuc)	*Renilla reniformis*	Coelenterazine	N/A	36	480
Renilla mutant (RLuc8)	*Renilla reniformis*	Coelenterazine	N/A	36	535
Gaussia (Gluc)	*Gaussia princeps*	Coelenterazine	N/A	20	470
NanoLuc (NLuc)	*Oplophorus gracilirostris*	Furimazine	N/A	19	460

*Modified from England, *et al*. 2016[4]

1.2 Autonomous bioluminescence systems

Autonomous bioluminescence (auto-bioluminescence) systems enable the monitoring of cellular events using bioluminescent probes without the addition of luciferin. In auto-

bioluminescence systems, several enzyme cascades are responsible for the production of luciferin. In other cases, the by-product of the luciferase chemical pathway, oxyluciferin, can be re-converted into luciferin by several enzyme cascades. Currently, there are two well-known systems that belong to auto-bioluminescence systems: bacterial and fungal bioluminescent systems[5,6]. Each auto-bioluminescence system also shows different physicochemical characteristics and pathways; however, bacterial luciferase has a thermostable and soluble characteristic[7] compared to fungal luciferase, which is preferable for application as a bioluminescent probe. As bioluminescent probes, the application of auto-bioluminescent systems, which have functions similar to those of common bioluminescent probes such as Fluc, Rluc, or Gluc in bioscience applications, especially for single-gene expression. For instance, applications of auto-bioluminescent as gene reporters with specific promoters for the detection of genotoxic agents[8], oxidative stress[9], signaling compounds, metabolites[10], and drug screening[11].

1.2.1 Fungal bioluminescence system

Fungal bioluminescence is a well-known auto-bioluminescence system which is first cloned from *Neonthopanus nambi* fungi[7]. In *N. nambi* fungal bioluminescence, four genes have been identified to promote auto-bioluminescence: *hisps* (hispidin synthase), *h3h* (hispidin-3-hydroxylase), *cph* (caffeylpyruvate hydrolase), and *luz* (luciferase). During the synthesis of luciferin (3-hydroxyhispidin), caffeic acid is converted to hispidin by HispS, followed by the conversion of hispidin to 3-hydroxyhispidin as luciferin by H3H. Luz then reacts with 3-hydroxyhispidin to emit light in the green spectrum (λ_{max}^{EM} ~520 nm) which produces oxyluciferin as caffeylpyruvic acid and followed recycling it into caffeic acid by CPH[6,7,12] (**Figure 1**).

Fungal luciferase has been expressed in several expression host, such as *E. coli*[7], mammalian cells (HEK293 cells)[7], yeast (*Pichia pastoris)*[7], and plant hosts[13,14]. However, auto-bioluminescence is fully functional only in plants and not in other hosts. It has been reported that bacteria, yeast, and mammalian cells cannot produce caffeic acid as a luciferin precursor; therefore, the initial addition of caffeic acid is mandatory to promote auto-bioluminescence systems[7]. In addition, the *N. nambi* Luz (nnLuz) protein has an N-terminal transmembrane helix that shows an insoluble fraction in *E. coli* and *P. pastoris*[12]. Recombinant nnLuz is optimally functional around pH 8.0 and moderate temperature and loses its activity above 30 ºC[7]. Thus, it is desirable to select other auto-bioluminescence systems that are thermostable and soluble for expression in multilevel organisms.

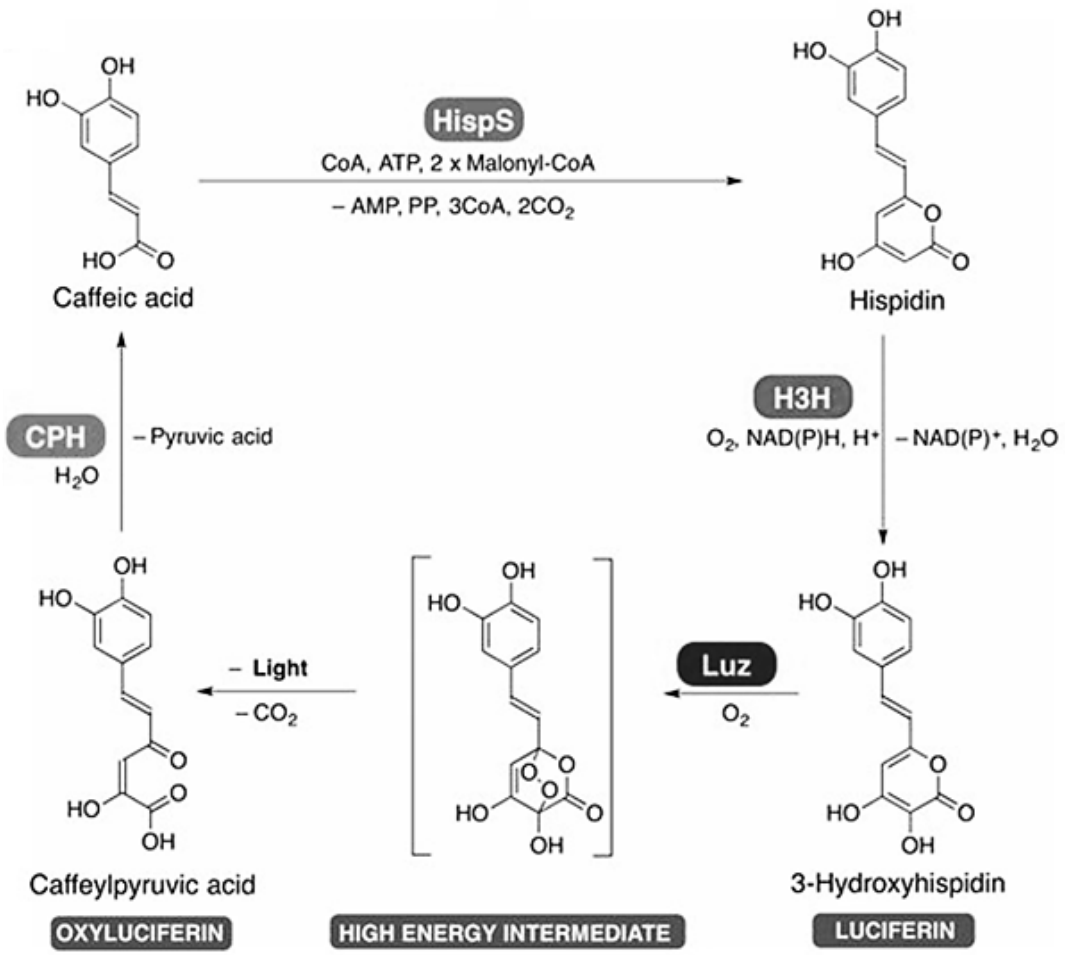

Figure 1. Reaction of fungal bioluminescence [7]**.**

1.2.2 Bacterial bioluminescence system

Bacterial bioluminescence is found in several species of the marine bacteria *Photobacterium* and *Vibrio*[15] and the soil bacterium *Photorhabdus*[16]. All of these bacterial luciferases emit the same spectrum with λ_{max}^{EM} ~490 nm by reacting of luciferase with reduced flavin mononucleotide ($FMNH_2$) and long-chain fatty aldehyde (RCOOH) as luciferin[17] (**Figure 2)**. Among these strains, *Photorhabdus* luciferase showed more thermostability than *Photobacterium* or *Vibrio* luciferase[16]. Thus, *Photorhabdus* luciferase is a promising probe for expression in mammalian hosts.

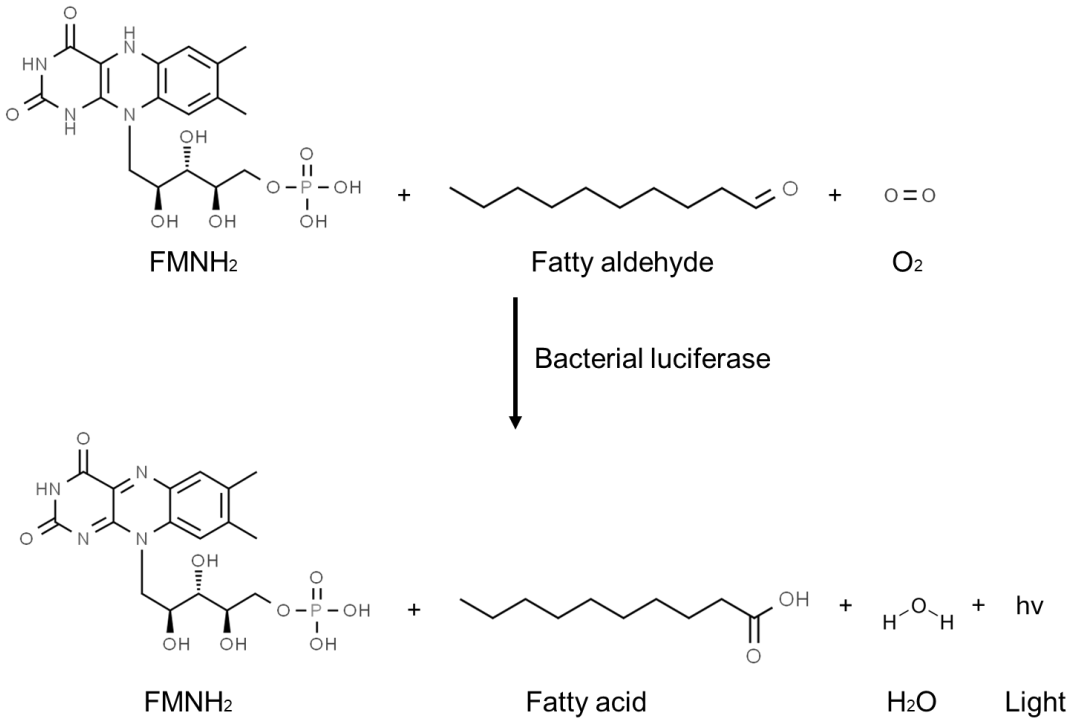

Figure 2. Bacterial bioluminescence reactions

Bacterial bioluminescence systems also belong to auto-bioluminescence systems, which genetically encode luciferase-luciferin production components. There are six genes to promote auto-bioluminescence: *luxA* and *luxB* (encode for the α and β subunits of bacterial luciferase), *luxC*, *luxD*, and *luxE* (encode for the synthesize of long-chain fatty aldehyde), and

the additional of *luxG* or *Frp* (encoded flavin reductase to provide $FMNH_2$ from FMN)[5], In the mechanism of bacterial luciferase to emit the light, the bacterial luciferase reacts with reduced FMN ($FMNH_2$/intermediate I). Intermediate I is produced by the reduction of oxidized FMN by an external FMN reductase, luxG or Frp. Intermediate I turns into intermediate II (FMN-4a-hydroxyperoxide) upon the reaction of luciferase-bound $FMNH_2$ with dioxygen. This intermediate is unstable in the absence of long-chain aldehydes and leads to intermediate III (FMN-4a-peroxyhemiacetal) after the binding of long-chain aldehyde and luciferase-bound intermediate II. The monooxygenation of intermediate III forms the excited state of FMN-4a-hydroxide, which serves as a bioluminophore. The excited state relaxes to the ground state and releases free energy as light and by-product fatty acids (R_2-COOH). After the release of one water molecule, the ground state of FMN-4a-hydroxide was oxidized to FMN[18] (**Figure 3**).

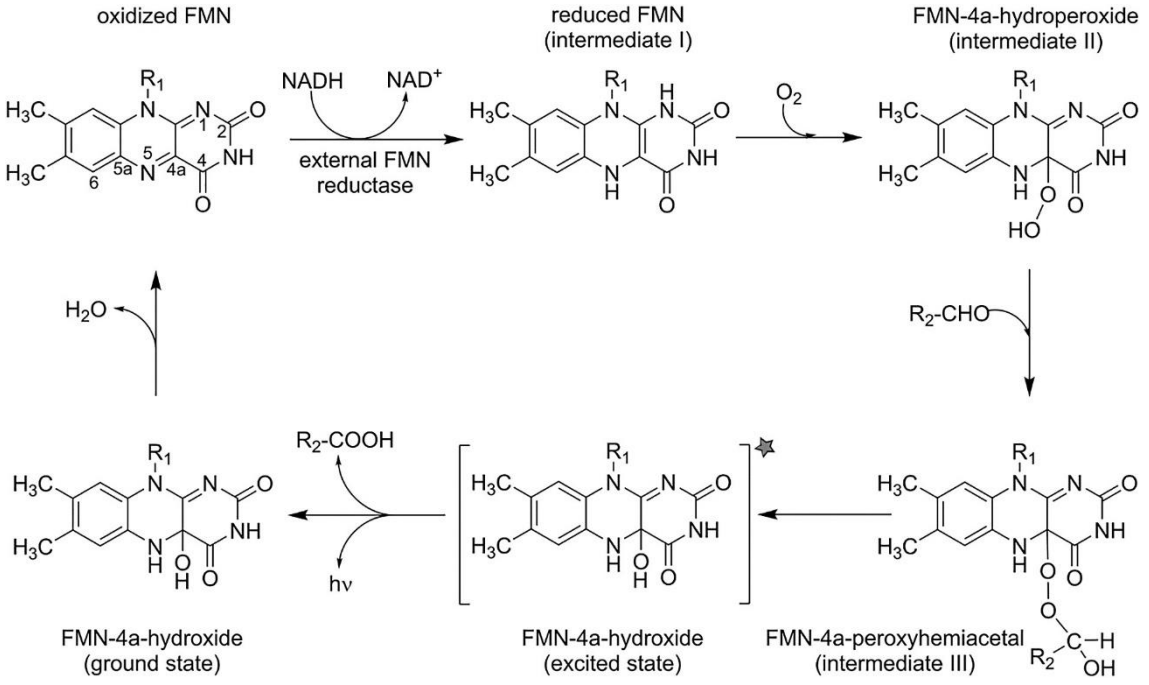

Figure 3. Catalytic mechanisms of bacterial luciferase[18].

Bacterial luciferases form heterodimeric proteins with the α- and β-subunits. The α subunit (40 kDa) contains the active site, whereas the β subunit (36 kDa) stabilizes LuxA[19]. Both α and β subunits have a TIM (β/α)8 barrel folding structure, which shares approximately 30% sequence identity and more than 95 of the 350 amino acids conserved[19]. In the crystal structure of *V. harveyi* luciferase (PDB: 3FGC), FMN binds to the active site of LuxA (α-subunit) in the side chains of Leu42, Glu43, Ala74, Ala75, Val77, Cys106, Arg107, Leu109, Tyr110, Agr125, Val173, Ala174, Glu175, Ser176, Thr179, and Trp192 (**Figure 4B**). The major deviation between LuxA and LuxB (β subunit) is that LuxA contains a 29-residue flexible loop near the active site cavity. This flexible loop protected the intermediate reaction (**Figure 4A**) from bulk solvent exposure [19,20].

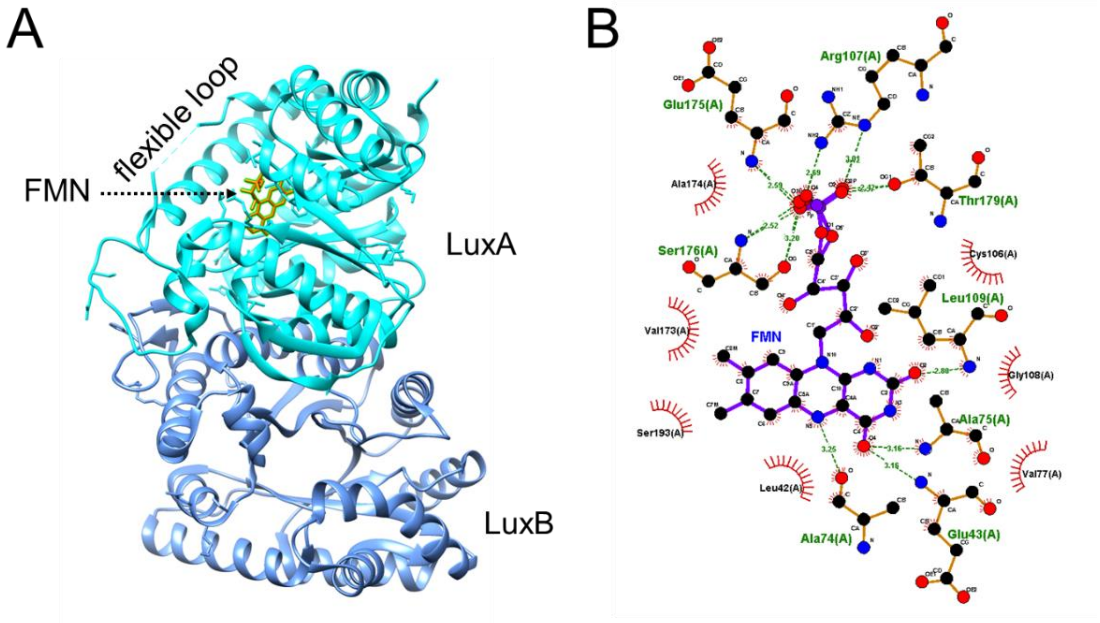

Figure 4. Crystal structure of bacterial luciferase (PDB: 3FGC) (A) and residues around the FMN-binding site (B).

The long-chain aldehyde is synthesized by the precursor of acyl-ACP or acyl-coA via enzyme cascades of the LuxCDE complex (**Figure 5A**). *luxD* encodes LuxD transferase, uses the acyl moiety of acyl-ACP or acyl-coA, and releases free fatty acids that interact with LuxE

synthetase (encoded by *luxE)*. The intermediate (acyl-AMP) produced from this step at the expense of ATP is reduced by LuxC reductase (encoded by *luxC*) with NADPH to long-chain aldehyde, where myristyl aldehyde (tetradecanal) is the main substrate in the luciferase reaction (**Figure 5B**)[18].

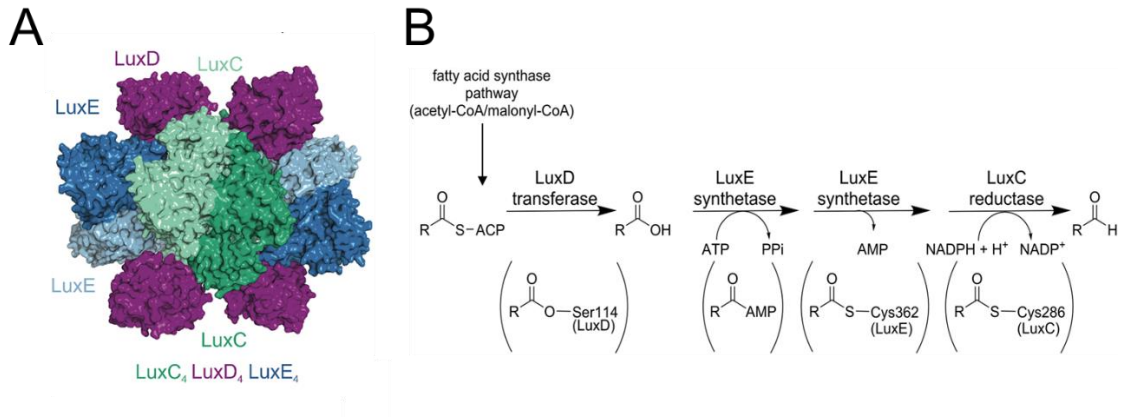

Figure 5. Model of the luxCDE fatty acid reductase complex (A) and catalyzed reactions (B)[18].

Bacterial luciferase commonly emits single color, blue-green (λ_{max}^{EM}~490 nm). Some bacterial strains emit light of different colors, such as yellow or blue. The marine bacterial strain *Photobacterium fischeri* Y-1 emits yellow light (λ_{max}^{EM}~545 nm) by forming a complex with yellow fluorescent protein YFP that binds FMN[21]. However, the color change is temperature-dependent, emitting yellow light at 18 ºC[22]. Another study found that *P. phosphoreum* can emit blue light (λ_{max}^{EM}~475 nm) by forming a complex with blue fluorescent protein (BFP, or lumazine protein/LumP). LumP uses lumazine as a chromophore synthesized by the rib/riboflavin operon (*ribABEH*)[23]. The mechanism by which both fluorescent proteins shift the emission light is speculated by the weak Förster resonance energy transfer (FRET). It has been suggested that the long-chain aldehyde is responsible for holding the luciferase and the fluorescent protein to shift the emission wavelength by the FRET phenomena[24]. Similar to

YFP-binding FMN, LumP protein is also affected by higher temperature[25]. Thus, a color-shifted bacterial luciferase with thermostability is necessary for further applications.

1.3 BRET-based bioluminescence systems

Resonance energy transfer (RET) is a phenomenon occurring between two photoactive molecules[26]. The energy is transfer from a donor to an acceptor molecule via a non-radiative resonance process through dipole-dipole coupling with proper distance and orientation. Subsequently, the spectrum wavelength of the donor changes to that of the acceptor. RET or FRET (Förster resonance energy transfer), from German scientist Theodor Förster, can be divided into two types: fluorescence RET (FRET)[26,27] and bioluminescence RET (BRET)[28,29], which use fluorescent and bioluminescent donors, respectively. The efficiency of RET transfer can occur only if the distance between the donor and acceptor is <10 nm and the orientation and spectrum overlap of the donor and acceptor[27].

In the case of BRET-based bioluminescence, previous lab members have developed the Nano-lantern (reminiscent of a light source with nanometer scale) series. The first report was a fusion of yellow fluorescent protein (Venus) with *Renilla luciferase* (Rluc) to yield YNL. The fusion changes the spectrum of Rluc (λ_{max}^{EM}~480) nm to λ_{max}^{EM}~530 nm[30]. The first Nano-lantern (YNL) was expanded by Takai, *et al*[31], who fused Rluc with mTurquoise2 and mKusabiraOrange2 to generate cyan (CNL) and orange (ONL) variants, respectively (**Figure 6A**).

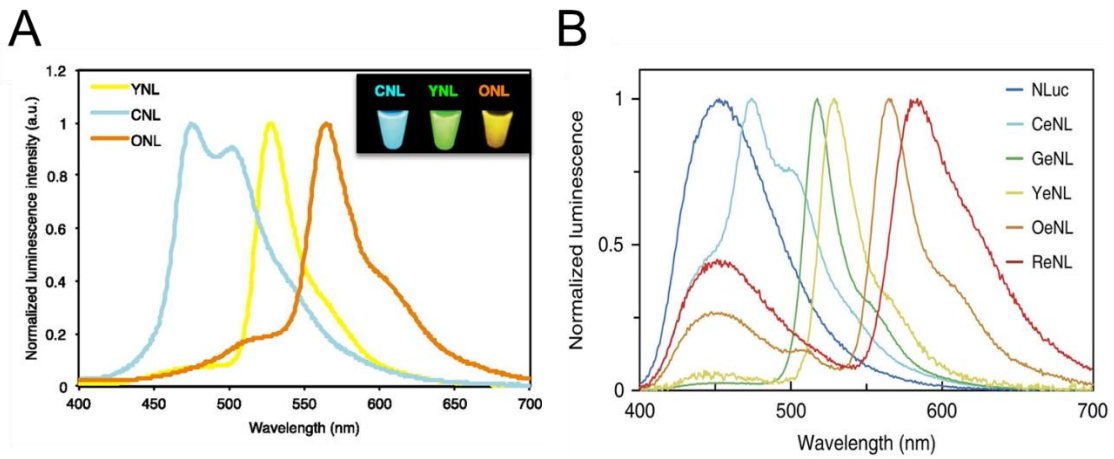

Figure 6. Spectral wavelengths of NLs (A)[31] and eNLs (B)[32].

Furthermore, Suzuki, *et al*[32] developed five color variants of NLuc by fusion with mTurquoise2, mNeonGreen, Venus, mKOk, and tdTomato to yield cyan eNL/enhanced Nano-lantern (CeNL), green eNL (GeNL), yellow eNL (YeNL), and red eNL (ReNL), respectively (**Figure 6B**). However, this recent Nano-lantern series used non-autobioluminescent types are limited to prolonged observation with multicolor bioluminescence imaging. Thus, it is challenging to develop multicolor bioluminescence imaging using auto-bioluminescence systems.

CHAPTER 2

DEVELOPMENT OF MULTICOLOR LUX

2.1 Introduction

Bioluminescence-based imaging has been widely used to observe biological phenomena in cells. To enable real-time imaging, common bioluminescence-based imaging requires continuous addition of luciferin to produce light. This can increase luciferin's autooxidation[33], lowering the signal-to-noise ratio and complicating long-term imaging. To overcome this issue, efforts have been made to produce luciferin-related genes to create auto-bioluminescence systems. As stated earlier, there are two auto-bioluminescence systems, such as bacterial luciferases (Lux) and fungal luciferases (Luz), but Luz is temperature-sensitive and has poor solubility[7], making Lux a more preferred option for auto-bioluminescent probes due to its physicochemical properties.

Auto-bioluminescence imaging based on Lux has been used for long-term imaging of single cells of bacteria (*E. coli*)[34] and mammalian cells[35]. However, when observing multiple biological events, auto-bioluminescence imaging based on Lux cannot be used because of the lack of distinct color variants compared with commonly modified non-autonomous luciferases[31,32]. Consequently, there is a considerable demand for Lux color variants to enable monitoring of diverse biological events. Previous color variants of Lux with a 4 nm shift in the emission spectrum of the wild-type Lux (λ_{max}^{EM}=534 nm) emerged as a result of mutations occurring in the active site of luciferase (LuxA) by introducing the A75G/C106V double mutation[36]. Color variants are also affected by protein-binding interactions of wild-type Lux with native yellow fluorescent protein (YFP)[37,38] and lumazine protein (LumP)[18,39]. Although

these strategies can shift the emission wavelength, that also perturb Lux activity, resulting in reduced luminescence[36] and thermostability[18,38,39].

To circumvent the limitations of the color variants of Lux, I adopted a BRET strategy inspired by Nano-lantern development, which successfully produced multicolor variants of luciferase without affecting its luminescence activity and thermostability. Here, I aimed to develop the first multicolor auto-bioluminescent Lux by fusing several FPs as BRET acceptors. This multicolor Lux can solve the problem of non-autonomous bioluminescence technology with limited application for long-term imaging of biological phenomena. I demonstrated this multicolor Lux for autonomous multiplexed imaging, which is expressible in bacterial, mammalian, and plant hosts.

2.2 Materials and methods

Gene construction. I used the luxAB operon in the pRSET$_B$ vector from Dr. Tomomi Kaku, a former laboratory member, as the starting material to develop multicolor Lux for *E. coli* expression. To create a fusion construct of BRET-based LuxA, I amplified the cDNAs of all fluorescent proteins (FPs) from pRSET$_B$ encoding mTQ2, sfGFP, Venus, mKOκ, mScarlet, mScarlet-I, CyOFP, and mCherry-XL by PCR and subcloned into the N-terminus of luxA in pRSET$_B$-luxAB with the addition of EL (glutamic acid-leucine) linkers using the TEDA method[40]. I deleted the C-terminus of the cDNAs' FPs mutants (FPsΔC10-luxAB), except mKOκ, by inverse PCR and circularized them using the TEDA method. To construct BRET-based LuxB, I amplified the FPsΔC10-luxAB fragments, except mKOκ, and subcloned them into the N- or C-terminus of LuxB in the pRSET$_B$ vector.

For mammalian expression, I obtained a human codon-optimized lux from co lux[35] to generate auto-bioluminescent mammalian cells. I subcloned the cDNA of FPs in NLXs into the N-terminus of co luxA in the pcDNA3.1(+) vector (Invitrogen) using the TEDA method. I fused the fusion of co luxB with co Frp by using the GGGGS linker using the TEDA method. For the 2A peptide, I fused P2A and T2A downstream of co luxD and co LuxE, respectively, to yield co luxD-P2A-co luxE-T2A in the pcDNA3.1(+) vector (Invitrogen), using the TEDA method. Subsequently, I fused luxC downstream of T2A from co luxD-P2A-co luxE-T2A to yield co luxD-P2A-co luxE-T2A-co luxC.

For plant expression, I subcloned NLXs-P2A-co luxBFrp and co luxD-P2A-co luxE-T2A-co luxC (DEC(KZK)) from pcDNA.1(+) into pRI201-AN (Takara Bio), which I linearized using *Sac*I and *Nde*I in MCS1 from the vector. I amplified the cDNAs of NLXs-P2A-co luxBFrp and co luxD-P2A-co luxE-T2A-co luxC fragments, which have overlapping regions with the pRI201-AN vector (in the *Sac*I and *Nde*I sites). I then ligated the constructs

using the TEDA method to yield NLXs-P2A- co luxBFrp/pRI201-AN and co luxD-P2A-co luxE-T2A-co luxC/pRI201-AN. To construct a single plasmid vector for plant expression, I subcloned co luxD-P2A-co luxE-T2A-co luxC/pRI201-AN into MCS2 of NLXs-P2A- co luxBFrp/pRI201-AN using the TEDA method. I transformed all the gene constructions into JM109(DE3) *E. coli* cells (Promega) for bacterial expression, and XL-10 Gold *E. coli* cells (Agilent Technologies) for mammalian and plan expression. I cultured in the Luria-Bertani (LB) medium with 100 μg/mL carbenicillin (Sigma-Aldrich) for bacterial and mammalian expression and 50 μg/mL kanamycin (Sigma-Aldrich) for plant expression at 37 ℃ for 10–12 h, and then, I performed plasmid purification.

Protein purification. I transformed *E. coli* strain JM109(DE3) (Promega) with the $pRSET_B$ plasmid harboring NLXs variants fused with an N-terminal polyhistidine tag by heat shock method at 42 °C for 45 s. I spread the transformants on an LB plate containing 100 μg/mL carbenicillin and incubated at 37 °C for overnight. I grew *E. coli* in a 200 mL LB medium containing 100 μg/mL carbenicillin at 23 °C for 60 h with gentle shaking at 120 rpm. I collected the *E. coli* cells by centrifugation, suspended them in phosphate buffered saline solution (PBS; Takara Bio) and ruptured using a French press (ThermoFisher Scientific). I purified the supernatant using Ni-NTA agarose affinity columns (Qiagen), washed it with 10 mM imidazole (FUJIFILM Wako) and eluted with 100 mM imidazole. Finally, I changed the buffer elution to 20 mM HEPES (pH 7.4) using a PD-10 column (GE Healthcare), quickly froze the protein solution in liquid nitrogen, and stored them at −80 °C.

Protein characterization. I performed luminescence characterization of recombinant proteins using the BNAH method[41]. I measured the luminescence intensity from 0.8 μM of luminescent

proteins and mixed them with 10 μM FMN, 20 μM decanal, and 100 μM BNAH (in an auto-dispenser) using a microplate reader (SH-9000, Corona Electric) with 1 s exposure. I then measured the emission spectra from 8 μM luminescent proteins of NLXs mixed with 10 μM FMN, 20 μM decanal, and 100 μM BNAH using a photonic multichannel analyzer PMA-12 (Hamamatsu Photonics) with 20 s exposure. To measure the luminescent quantum yields, I measured the values from the total light output by the complete consumption of 20 nM decanal using a microplate reader (SH-9000, Corona Electric) with 0.1 s exposures. I determined the photon count of the microplate reader detector using the luminol photon calibration method as reported previously[42]. The final concentrations of the proteins, FMN, and BNAH were 200 nM, 10 μM, and 100 μM BNAH (in an auto-dispenser). For kinetic parameters, I used 200 nM of proteins with final decanal concentrations of 0.01, 0.1, 0.5, 1, 5, 10, 50, and 80 μM. I measured the initial reaction velocities as the luminescence intensities for the initial 10 s and fitted to the Michaelis-Menten equation using Origin8 (OriginLab) software to estimate the Michaelis-Menten constants (K_m) and maximum reaction velocities (V_{max}). To generate the k_{cat} values, I calculated it by dividing V_{max} by the quantum yield and number of luciferase molecules. All experiments were performed at 37^{o}C and performed in triplicate. The averaged data were used for further analysis.

Mammalian cell culture and transfection. I cultured HEK293T cells in Dulbecco's Modified Eagle's Medium (DMEM) (Sigma-Aldrich) supplemented with 10% fetal bovine serum (FBS; Biowest) at 37 °C in 5% CO_2. I seeded cells on collagen-coated 35 mm glass-bottom dishes or 12-well dishes. For transfection, I transfected the recombinant DNA using polyethylene imine (PEI Max 40 K; Polyscience), according to the manufacturer's instructions. The final concentration of all plasmids transfected was one μg/mL. In the case of six series of co lux, the

total plasmids of co-transfected follow from the previous report[35] with a mixture of 83 ng co luxA, 83 ng co luxB, 83 ng co Frp, 250 ng co luxC, 250 ng co luxD, and 250 ng co luxE plasmids. I cultured the cells for ~48 h and exchanged the medium with phenol red−free DMEM/F12 (ThermoFisher Scientific) and used it for imaging or assay.

Transient expression in *Nicotiana benthamiana* leaves by *Agrobacterium* infiltration. For plant expression, I transformed the plant expression plasmids into *Agrobacterium tumefaciens* (GV3101) and cultured overnight on a shaker at 28 °C in LB medium with kanamycin selection. I collected the bacterial cultures and resuspended in infiltration buffer (10 mM $MgCl_2$, 10 mM MES pH 5.6, and 200 μM acetosyringone) to OD_{500} = 0.6. I kept the suspension at room temperature in the dark for 2 h. I infiltrated the suspension using a needleless syringe to the abaxial side of *the N. benthamiana* leaves (5-6 weeks old). Three days after infiltration, I observed bioluminescence activity.

Bioluminescence imaging. For the luminescence image of NLXs expressed in *E. coli* colonies, I used SONY α7s (ISO 20000, for 10s of exposure in the LB plates. To perform single-cell imaging of NLXs, I mixed recombinant *E. coli* expressing CNLX, YNLX, and RNLX in LB plates into 10 μL of H_2O. I introduced the 0.3 μL of each recombinant *E. coli* into 35 mm glass bottom dishes using the agar pad method. I performed microscopy luminescence imaging with an inverted microscope based on the IXplore™ Live system equipped with an EM-CCD camera (Andor iXon Ultra 888) with 8 min of exposure, EM-gain of 1000×, ×100 objective lens and 2 × 2 binning settings. Three filters, Olympus U-FCFP (460-510), Olympus U-FYFP (515-560), and Olympus U-FMCHE (600-690), were used to separate *E. coli* images.

For luminescence imaging of auto-bioluminescence NLXs expressed in HEK293T cells, I acquired them with an inverted microscope based on the IXplore^{TM} Live system equipped with an x40 objective lens (Olympus, UPlanSApo, numerical aperture 1.4). The emission signals were detected by an EM-CCD camera (Andor iXon Ultra 888) with 60s of exposure. I used five filters, consist of Olympus U- Olympus FCFP (460-510), Semrock FF01-514/30 (510-550), Olympus U-FYFP (515-560), Semrock FF01-562/40, and Olympus U-FMCHE (600-690), to separate NLXs images. For mixed HEK293T cells expressing CNLX, YNLX and RNLX, I used three filters consist of Olympus U- FCFP (460-510), Olympus U-FYFP (515-560), and Olympus U-FMCHE (600-690), to separate the mixed cell images. For luminescence imaging of auto-bioluminescent NLXs expressed in *N. benthamiana* leaves, I observed bioluminescence activity using a DSLR-based camera (SONY α7s, ISO 20000) with 60 s of exposure and a CCD-based camera (Vilber Fusion FX) with 1-60 s of exposure.

Quantitative analysis of NLXs and nnLuz genes. I homogenized *N. benthamiana* leaves expressing NLXs and nnLuz with metal beads, and I extracted the total RNA using NucleoSpin® RNA Plant (Takara Bio). I performed reverse transcription of one microgram of total RNA to first-strand cDNA using ReverTra Ace™ qPCR RT Master Mix (Toyobo). I then performed real-time quantitative RT-PCR on a StepOne Real-Time PCR system (Thermo Fisher Scientific) using PowerUp SYBR Green Master Mix (Thermo Fisher Scientific). I calculated the baseline, threshold cycles (CT), and comparative CT (ΔΔCT) using StepOne software v2.3, normalized by PP2A39 gene expression, and analyzed the relative gene expression by comparative CT (ΔΔCT).

Modelling, data analysis and statistical methods. I used the amino-acid sequence of LuxAB from *Photorhabdus luminescencs* as input for the Alphafold2 structure prediction[43] in the ColabFold server. I visualized the three-dimensional structures of protein using UCSF-chimera[44].

I analyzed all bioluminescent images from the microscope using ImageJ and MetaMorph software. I subtracted the bioluminescence images of the microscope from the background, and the cosmic rays were processed with an adaptive median filter without affecting the original brightness or morphology of the cells using ImageJ software. I used the pseudocolor images for microscopy images with "Red Hot" color for total luminescence intensity and a specific color for each cell according to specific wavelengths.

I performed data fitting and statistical analysis using Origin8 (OriginLab). I performed statistical analysis using unpaired Student's t-test for comparing two parameter sets, and I used one-way ANOVA followed by post hoc Tukey's honestly significant difference test to compare more data sets.

2.3 Results and discussion

2.3.1 Development Nano-lantern based on Lux (NLX)

I adopted a BRET strategy to change Lux's bioluminescence color, First, I used the yellow fluorescent protein (FP) Venus[45] as the initial BRET acceptor protein (**Figure 7**). The effects of BRET with Venus, including modifications, were verified as previously reported[46]. I fused Venus to the N- or C-terminus of the active subunit of Lux (LuxA) to achieve higher BRET efficiency (**Figure 8A).** To compare the bioluminescence intensities of these fusion proteins without the influence of endogenous FMN levels, I measured them in purified proteins, not in cell systems, as previously reported[46]. For bioluminescence measurements, I added the purified Lux and Venus fusions to the FMN, decanal, and BNAH[41]. I found that the intensities of these fusions were lower than those of wild-type Lux (**Figure 8B).** I speculated that unstructured residues from the C-terminus of Venus might affect the activity or protein folding of LuxA. Consequently, I found that the deletion of the C-terminus of Venus (VenusΔC10-LuxA) significantly improved the bioluminescence intensity compared to the wild-type (**Figure 8B).**

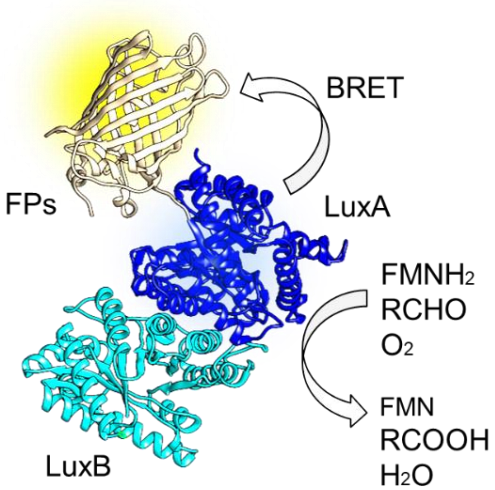

Figure 7. Structural model of NLX. The structural model consisted of heterodimeric Lux, LuxA (blue), LuxB (cyan), and FP (yellow).

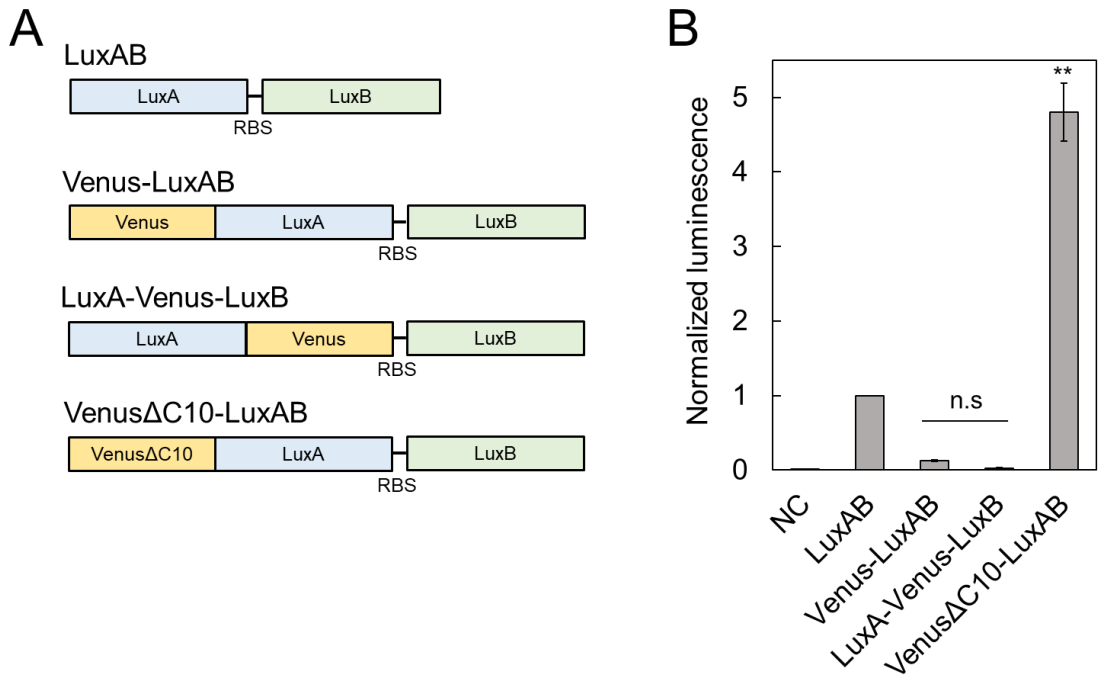

Figure 8. Optimization of Venus fusion position to LuxA. (A) Schematic representation of the Venus fusion position to the LuxAB operon. The RBS is a ribosome-binding site. **(B)** Bioluminescence intensity from equimolar amounts with or without C-terminal deletion of Venus fused to LuxA**.** NC is HEPES solution without LPs. $n = 3$, $^{**}p < 0.05$.

Referring to this structure, I fused the LuxA with other FPs, including mTurquoise2[47] (cyan FP), sfGFP[48] (green FP), and mKOκ[49] (orange FP), to serve as BRET acceptors **(Figure 9A)**. As a result, these fusions changed the luminescence color and shifted the emission wavelength compared to the original lux (**Figure 9A-B**). I designated these fusions as NLX (**N**ano-**l**antern based on Lu**x** luciferase), consisting of cyan NLX (CNLX) (λ_{max}^{EM}=480 nm), green NLX (GNLX) (λ_{max}^{EM}=520 nm), yellow NLX (YNLX) (λ_{max}^{EM}=534 nm), and orange NLX (ONLX) (λ_{max}^{EM}=569 nm). In the development of the red variant, I carried out the optimization of red FPs variants because of the lower spectral overlap between Lux and common red FPs. I selected mScarlet-I[50] as and red NLX (RNLX) (λ_{max}^{EM}=597 nm) due to its

higher BRET efficiency compared to CyOFP1[51], mCherry-XL[52], and Scarlet[50] (**Figure 10A-B** and **Table 2**). I also attempted to fuse FPs with the N- or C-terminus of LuxB to assess their suitability for LuxB fusion[46], aiming to produce a multicolor Lux. Even then, the BRET efficiency of the LuxA fusion was higher than that of the LuxB fusion (**Figure 11** and **Table 3**).

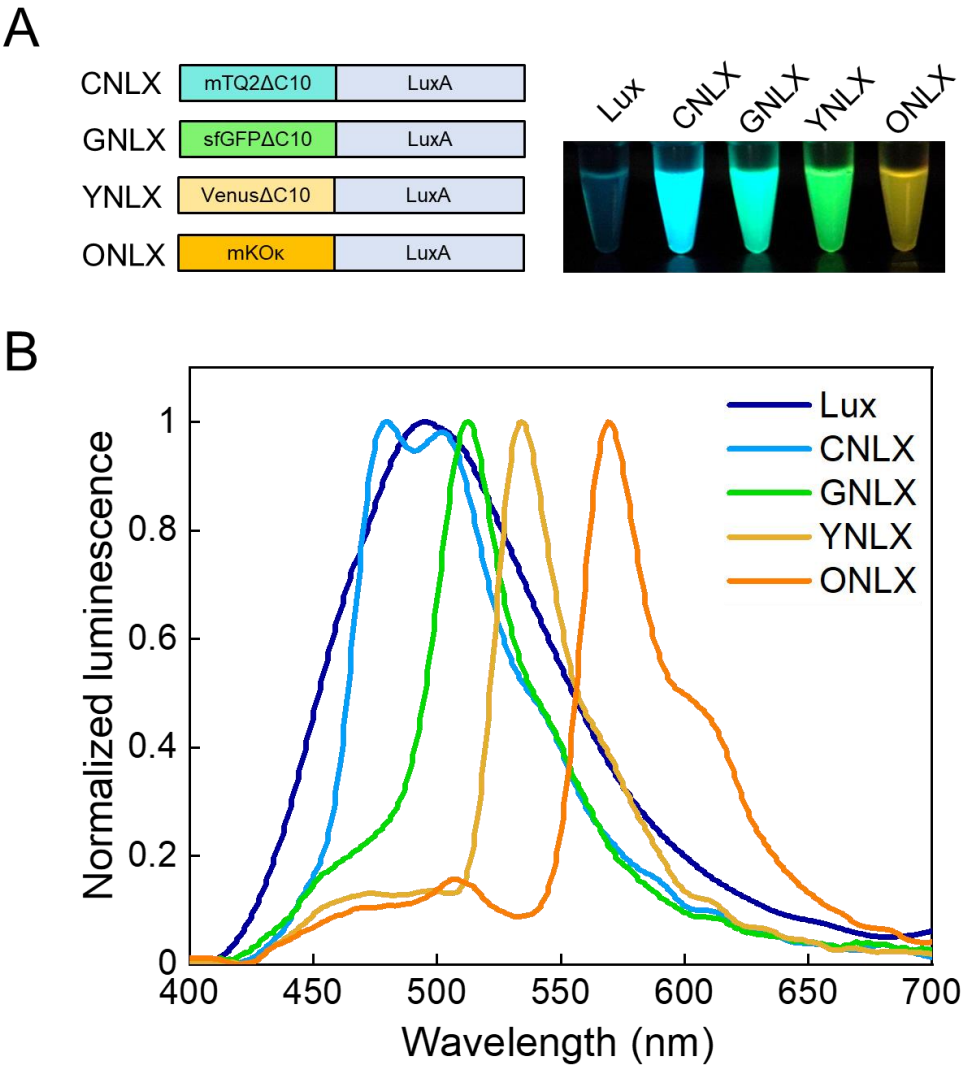

Figure 9. Schematic (A) and bioluminescence spectra of CNLX, GNLX, YNLX, and ONLX (B). (A) NLXs gene schematic (upper panel) and bioluminescence images of recombinant NLXs proteins (lower panel). **(B)** Bioluminescence spectra were normalized to each peak intensity.

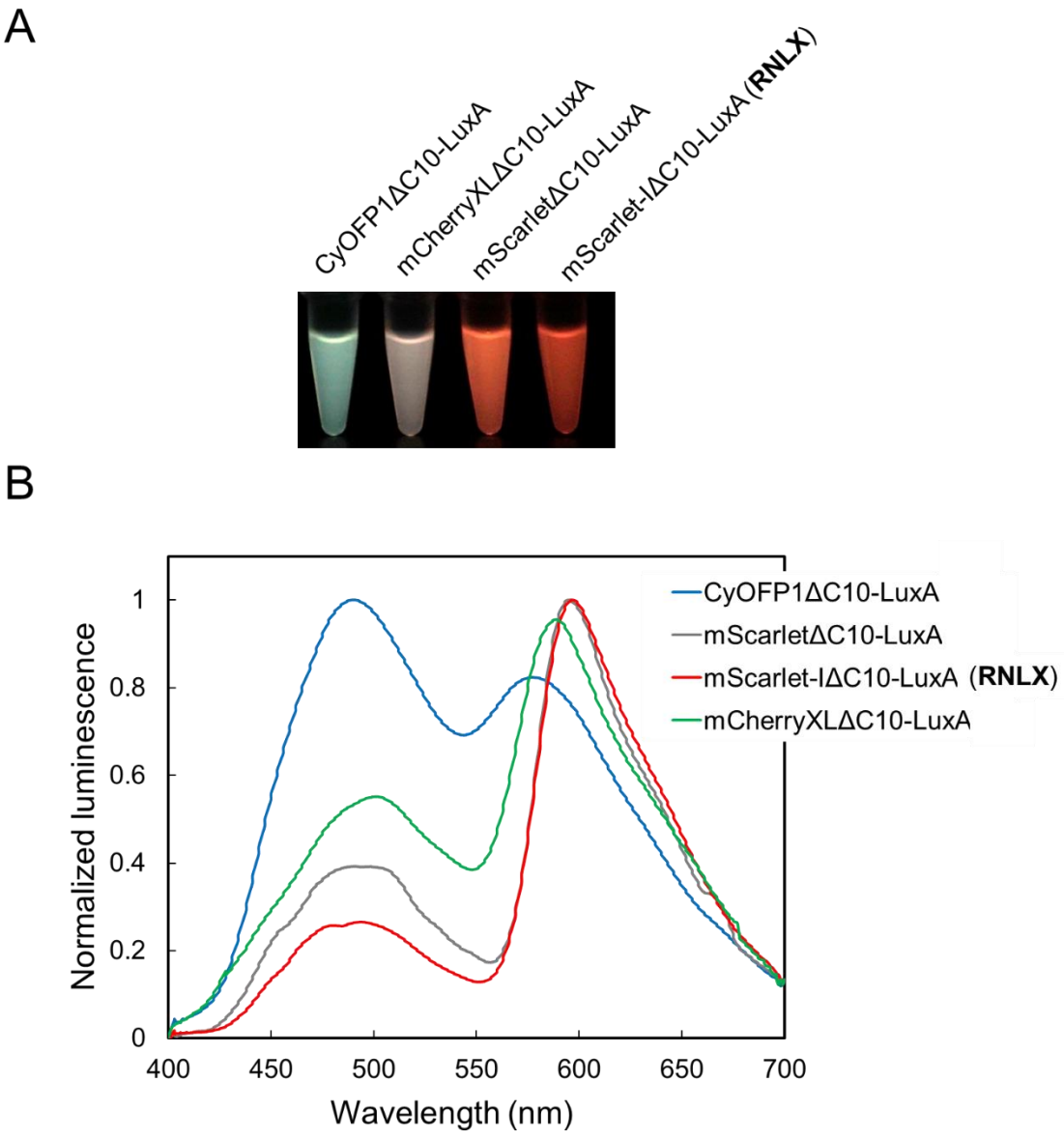

Figure 10. Optimization of red variants Lux. (A) Bioluminescence images of the recombinant proteins. **(B)** Bioluminescence spectra of optimization for red variants of NLXs. Bioluminescence intensities are normalized by peak intensity.

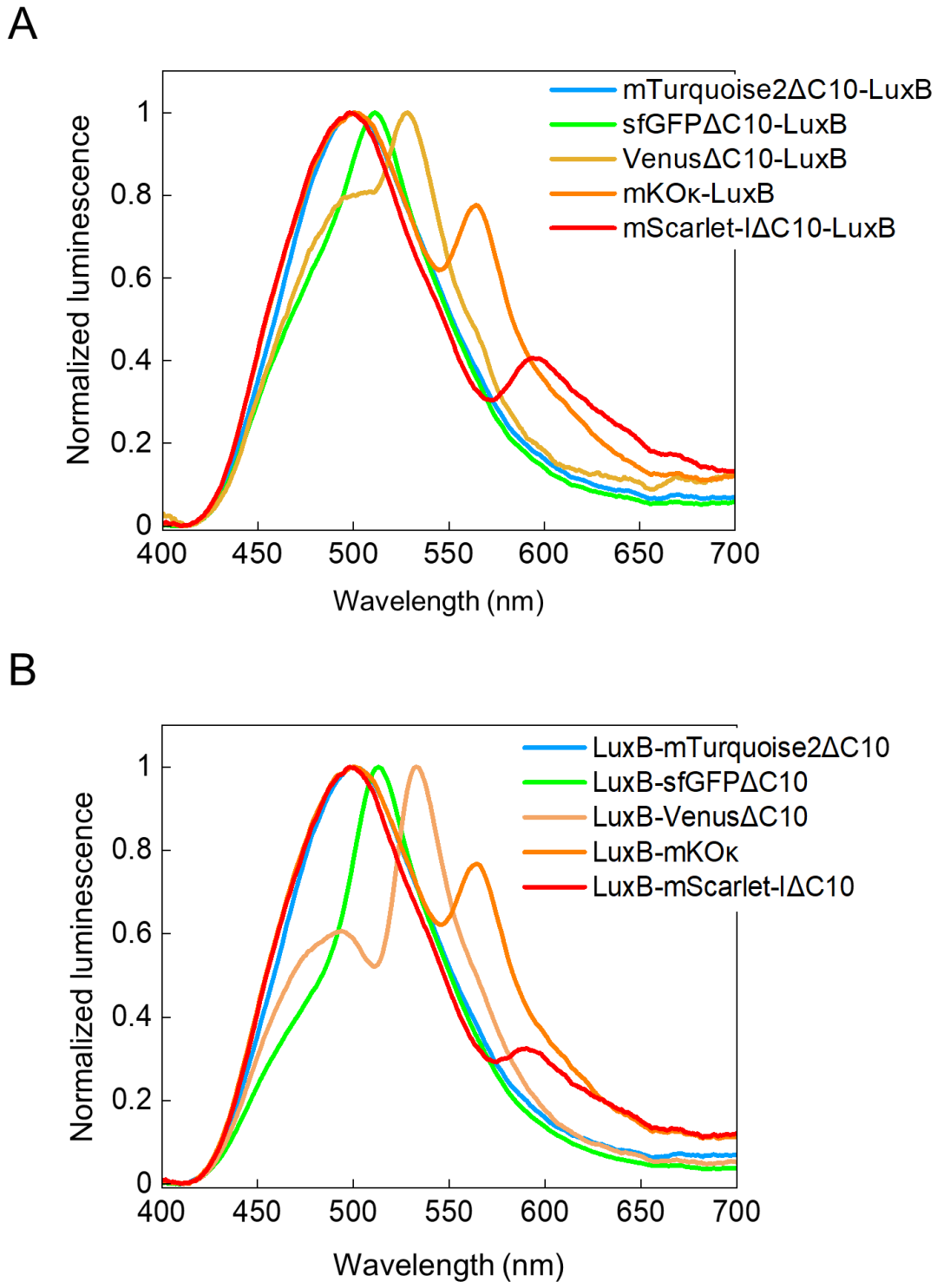

Figure 11. Fluorescent protein fusion to the N- or C-terminus of LuxB. Emission spectra of fluorescent proteins fused to the N-(**A)** or C-terminus **(B)** of LuxB**.** Bioluminescence intensities are normalized by peak intensity.

Table 2. Apparent BRET efficiency of LuxA proteins.

LPs	$\boldsymbol{I_{acceptor}/I_{donor}}$
mTurquoise2ΔC10-LuxA (CNLX)	1.06
sfGFPΔC10-LuxA (GNLX)	2.63
VenusΔC10-LuxA (YNLX)	7.69
mKOκ-LuxA (ONLX)	8.85
mScarlet-IΔC10-LuxA (RNLX)	3.85
CyOFP1ΔC10-LuxA	0.80
mCherryXLΔC10-LuxA	1.79
mScarletΔC10-LuxA	2.56

Comparison of BRET efficiency of BRET Lux proteins shown in **Figure 9** and **Figure 10**. The BRET efficiency was measured by the ratio of luminescence intensities of the acceptor peak ($I_{acceptor}$) to that of the donor peak (I_{donor}).

Table 3. Apparent BRET efficiency of LuxB proteins.

LPs	$\boldsymbol{I_{acceptor}/I_{donor}}$
mTurquoise2ΔC10-LuxB	0.84
sfGFP2ΔC10-LuxB	1.33
VenusΔC10-LuxB	1.17
mKOκ-LuxB	0.68
mScarlet-IΔC10-LuxB	0.47
LuxB-mTurquoise2ΔC10	0.82
LuxB-sfGFP2ΔC10	1.68
LuxB-VenusΔC10	1.54
LuxB-mKOκ	0.85
LuxB-mScarlet-IΔC10	0.49

Comparison of BRET efficiency of BRET Lux proteins shown in **Figure 11**. The BRET efficiency was measured by the ratio of luminescence intensities of the acceptor peak ($I_{acceptor}$) to that of the donor peak (I_{donor}).

Subsequently, to validate the universality of the NLX strategy across different Lux strains, I implemented the NLX approach on another strain of LuxA, *Photobacterium leiognathi* LuxA (*Ple*Lux)[53]. This LuxA variant shares 75.6% amino acid similarity[53] with *Photorhabdus luminescens* LuxA (this study). As a result, *Ple*Lux fusion (*Ple*NLX) produced a wavelength that was comparable to that of the original NLXs (**Figure 12).** However, the BRET efficiency of *Ple*NLX, particularly for the orange and red variants, was lower than that of the original NLXs (**Table 4**). Overall, the NLXs strategy was successful and broadly generated multicolor Lux.

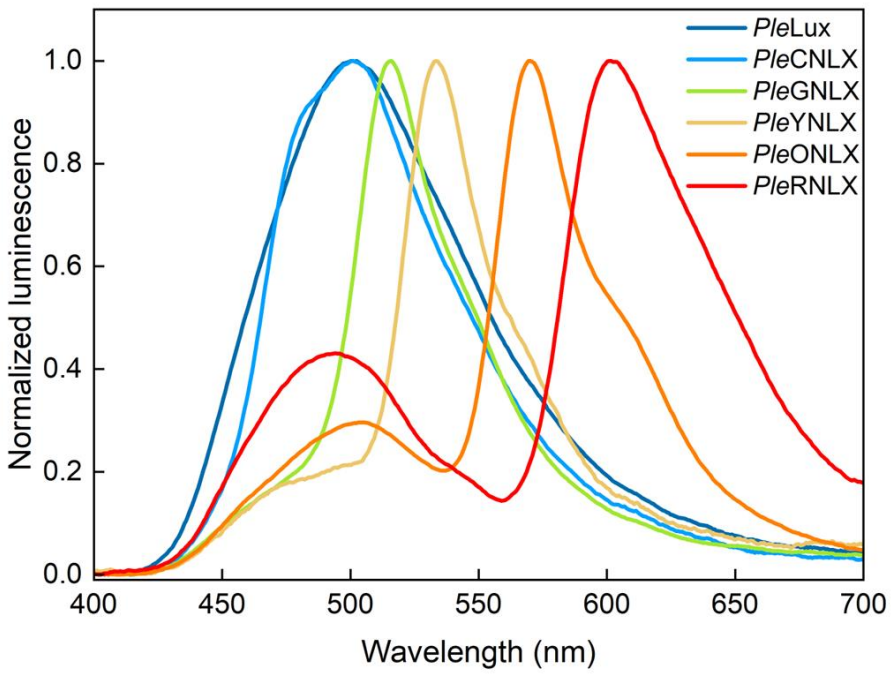

Figure 12. NLXs emission spectra of *Photobacterium leiognathi* LuxA. Emission spectra of fluorescent proteins fused to the N-terminus of *Photobacterium leiognathi* LuxA (*Ple*Lux). Fluorescent protein fusion followed the same strategy as that used for the original NLXs. Data were measured in triplicate and are presented as the mean and normalized at peak intensity.

Table 4. Apparent BRET efficiency of LuxA proteins.

LPs	$I_{acceptor}/I_{donor}$
mTurquoise2ΔC10-*Ple*LuxA (*Ple*CNLX)	0.84
sfGFPΔC10-*Ple*LuxA (*Ple*GNLX)	3.49
VenusΔC10-*Ple*LuxA (*Ple*YNLX)	5.19
mKOκ-*Ple*LuxA (*Ple*ONLX)	3.35
mScarlet-IΔC10-*Ple*LuxA (*Ple*RNLX)	2.27

Comparison of BRET efficiency of BRET Lux proteins shown in **Figure 12**. The BRET efficiency was measured by the ratio of luminescence intensities of the acceptor peak ($I_{acceptor}$) to that of the donor peak (I_{donor}).

2.3.2 *In vitro* characterization of NLXs

I found that the bioluminescence intensities of the purified NLXs were higher than that of the original Lux (**Figure 13**). I next examined the effect of FPs fusion, which can increase the bioluminescence intensity, by quantum yield and enzymatic kinetic measurements. The fusion of FP increased the luminescent quantum yield (QY) (**Figure 14A)**, whereas the enzymatic parameters (k_{cat}) of all NLXs were similar to those of wild-type Lux (**Figure 14B** and **Table 4**). As reflected by the emission intensity, the QY of CNLX was six times higher than that of Lux (**Table 4**).

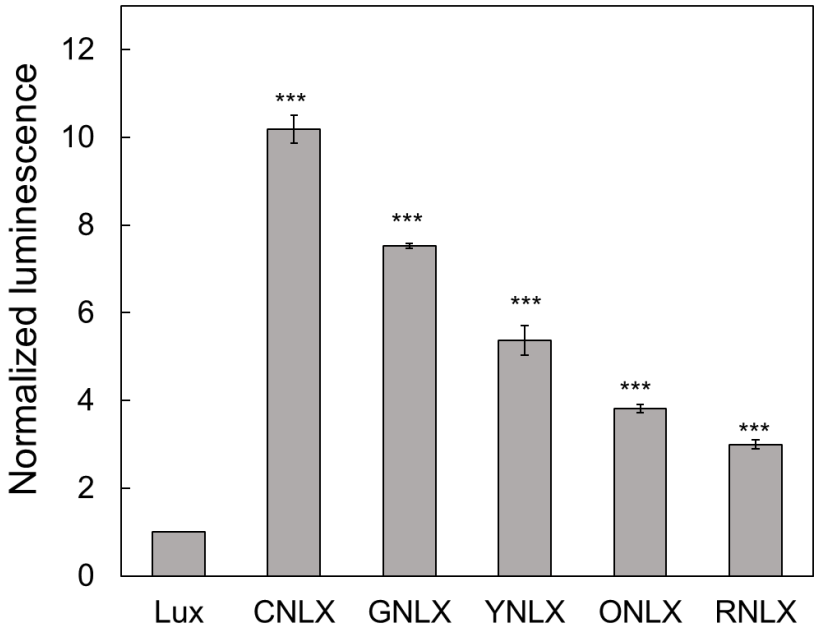

Figure 13. Bioluminescence spectra intensities of NLXs. Comparison of bioluminescence intensities of NLXs proteins and Lux. Data are mean ± s.d. $n = 3$, ***$p < 0.001$

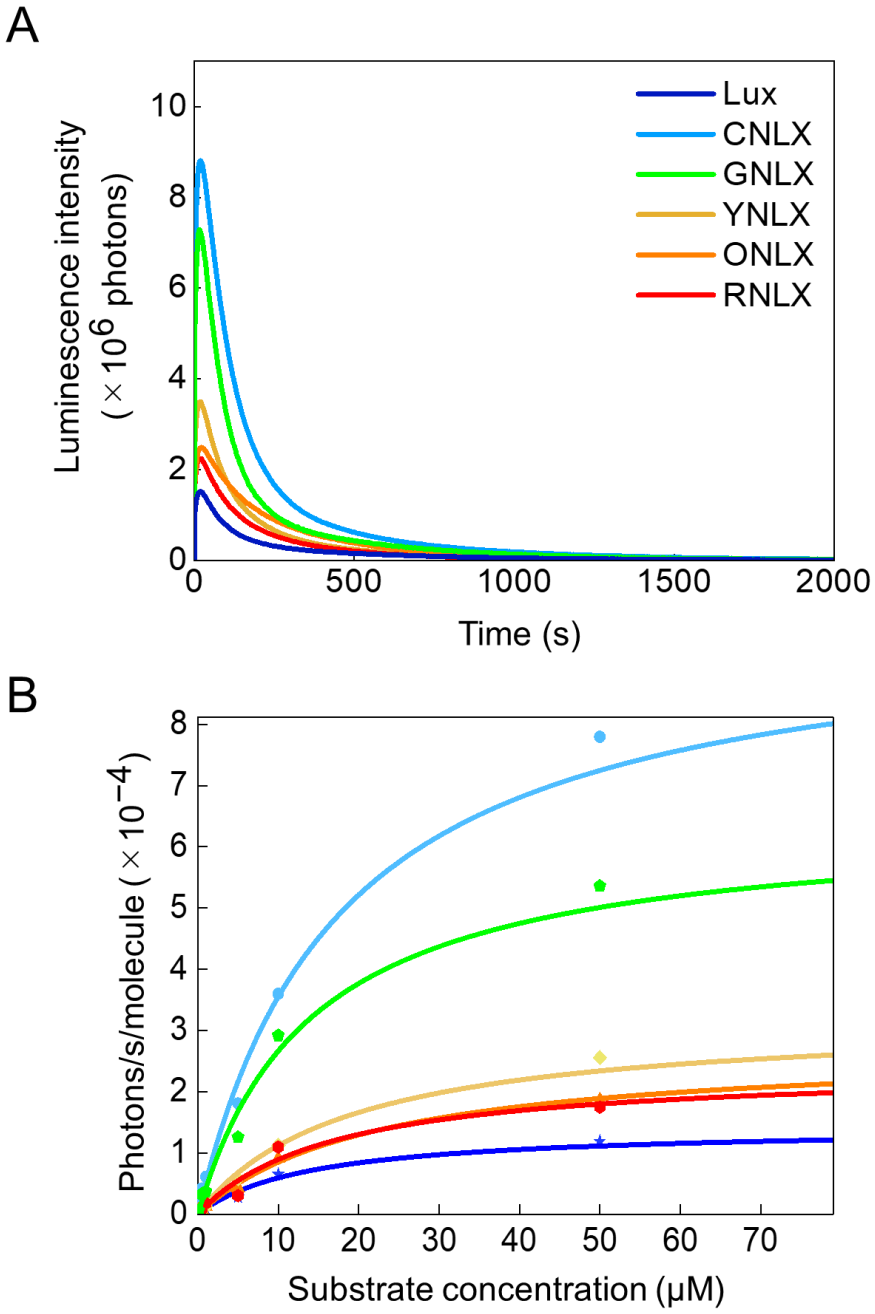

Figure 14. LPs characterization. (A) Quantum yield (QY) measurements of NLXs. The QY was estimated from the integrated light output until the reaction of the substrate, decanal, approached completion. **(B)** Enzyme kinetics of the NLXs**.** Kinetics parameters were estimated from the plot of the initial light output vs. the concentration of the decanal. The results are summarized in **Table 4**.

Table 4. Enzymatic characteristics of luminescent proteins.

LPs	LQY	K_m (μM)	V_{max} (photon s^{-1} $molecule^{-1}$)	k_{cat} (s^{-1})
Lux	0.11 ± 0.01	30.48 ± 15.10	$1.47 \times 10^{-4} \pm 1.72 \times 10^{-5}$	$1.24 \times 10^{-3} \pm 1.45 \times 10^{-4}$
CNLX	0.64 ± 0.05	23.46 ± 7.74	$9.43 \times 10^{-4} \pm 3.48 \times 10^{-5}$	$1.58 \times 10^{-3} \pm 1.32 \times 10^{-4}$
GNLX	0.45 ± 0.03	24.58 ± 8.21	$6.61 \times 10^{-4} \pm 7.74 \times 10^{-5}$	$1.47 \times 10^{-3} \pm 1.72 \times 10^{-4}$
YNLX	0.27 ± 0.01	25.74 ± 6.74	$3.66 \times 10^{-4} \pm 3.99 \times 10^{-5}$	$1.35 \times 10^{-3} \pm 1.47 \times 10^{-4}$
ONLX	0.23 ± 0.01	40.91 ± 17.25	$3.49 \times 10^{-4} \pm 1.31 \times 10^{-4}$	$1.49 \times 10^{-3} \pm 5.60 \times 10^{-4}$
RNLX	0.18 ± 0.02	31.42 ± 12.61	$3.64 \times 10^{-4} \pm 1.16 \times 10^{-4}$	$1.82 \times 10^{-3} \pm 3.95 \times 10^{-4}$

LQY, luminescent quantum yield. Data are presented as mean ± s.d., n = 3.

2.3.3 Auto-bioluminescence imaging of NLXs in live *Escherichia coli* cells

I evaluated the co-expression of NLXs with luciferin biosynthesis genes, *luxCDE*, to promote multicolor auto-bioluminescence in *Escherichia coli* (*E. coli*). I transformed *E. coli* with NLXs and the *luxCDE* operon, both driven by the T7 promoter. The data showed that the bioluminescence emitted by recombinant *E. coli* expressing individual NLXs exhibited the expected colors, consistent with the bioluminescence observed in NLX-purified proteins (**Figure 15**).

Additionally, I performed multiplexed auto-bioluminescence single cells imaging by mixing *E. coli* containing CNLX, YNLX, and RNLX plasmids (**Figure 16**). Recombinant *E. coli* demonstrated the capacity to be differentiated by color, using specific optical filters, and minimizing spectral noise with spectral unmixing algorithms[54]. This study marks the first report of multicolor auto-bioluminescent bacteria with a large spectral range from blue to red.

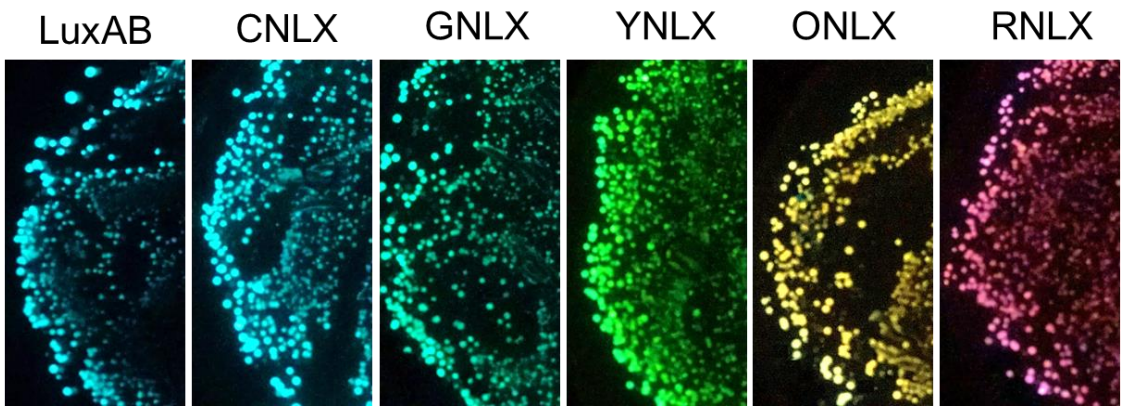

Figure 15. Auto-bioluminescence images of NLXs in live *E. coli* cells. Auto-bioluminescence images of *E. coli* expressing all NLX variants. Bioluminescence images were acquired using a Sony α7s camera.

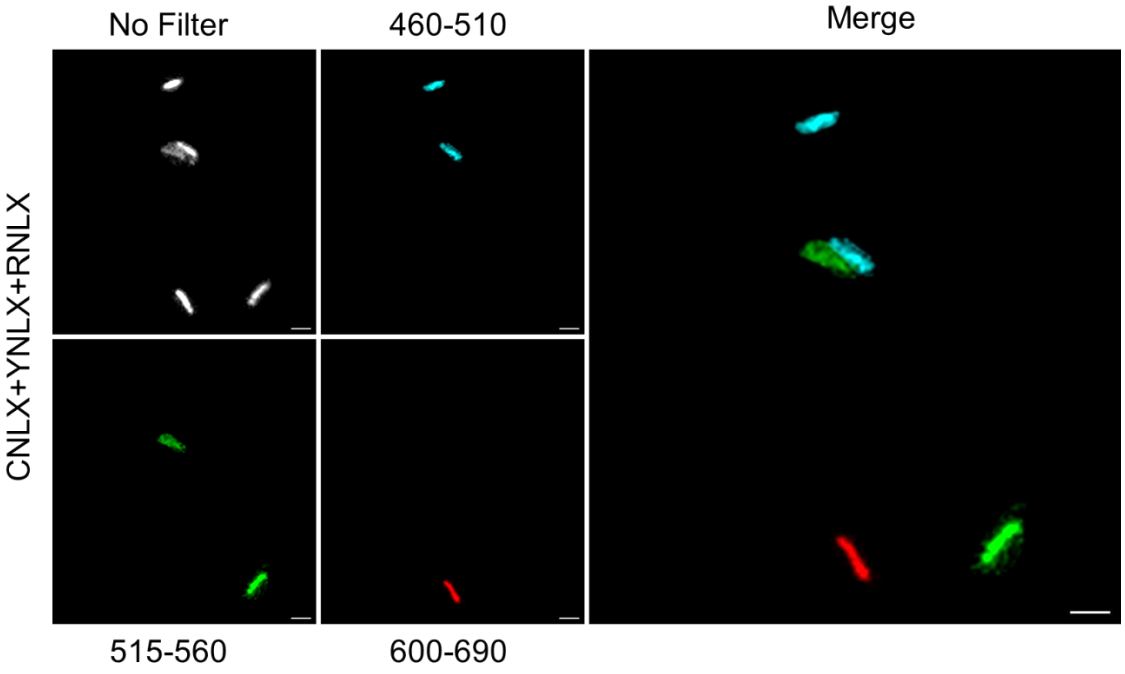

Figure 16. Single-cell auto-bioluminescence imaging of NLXs in live *E. coli* cells. Auto-bioluminescence imaging of mixed *E. coli* expressing CNLX, YNLX, or RNLX. Scale bars, 2 μm: ×100 magnification.

2.3.4 Auto-bioluminescence imaging of NLXs in live HEK293T cells

I next evaluated NLXs' performance in mammalian cells, HEK293T cells, by introducing it into the human codon-optimized lux operon (co luxA, co luxB, co luxC, co luxD, co luxE, and co Frp)[35], replacing luxA in NLXs with co luxA. Since the original co lux expression necessitated co-transfecting six plasmids for each gene, I sought to minimize the number of plasmids by utilizing the 2A peptide to link proteins (**Figure 17A**). I constructed co luxD, co luxE, and co luxC as a tricistronic unit using two 2A peptides (luxD-P2A-co luxE-T2A-co luxC) (DEC(2A)). In addition, I fused co luxB with co Frp using GGGGS (G4S)[55]. As a result, the fusion of co luxB and co Frp, BF(G4S), increased the luminescence intensity in cells compared to that of co lux (**Figure 17B**). In contrast, DEC(2A) did not enhance the intensity, which was also similarly reported previously[35], Therefore, by introducing the Kozak sequence[56] downstream of the 2A peptide, DEC(KZK) (**Figure 17A**), the luminescence intensity was improved (**Figure 17B**).

For mammalian expression, I used the optimized co lux operon-expressing plasmids, BF(G4S) and DEC(KZK), in this study. I confirmed the luminescence of the introduced NLXs by microscopy using an EM-CCD camera for single-cell imaging. The data showed that each luminescence color could be separated using specific optical filters (**Figure 18**). Subsequently, I performed multiplex auto-bioluminescence imaging by mixing HEK293T cells expressing CNLX, YNLX, and RNLX (**Figure 19A**). Similar to the mixed *E. coli* results, the cells could be distinguished by their respective wavelengths using spectral unmixing. I also conducted multiplex auto-bioluminescence imaging of subcellular structures by fusing RNLX with histones (H2B-RNLX) and YNLX with the plasma membrane (Lyn-YNLX), expressing them in HEK293T cells (**Figure 19B**). As a result, I could separate the luminescence signals from H2B-RNLX and Lyn-YNLX by optical filtering and successfully showed correct localization.

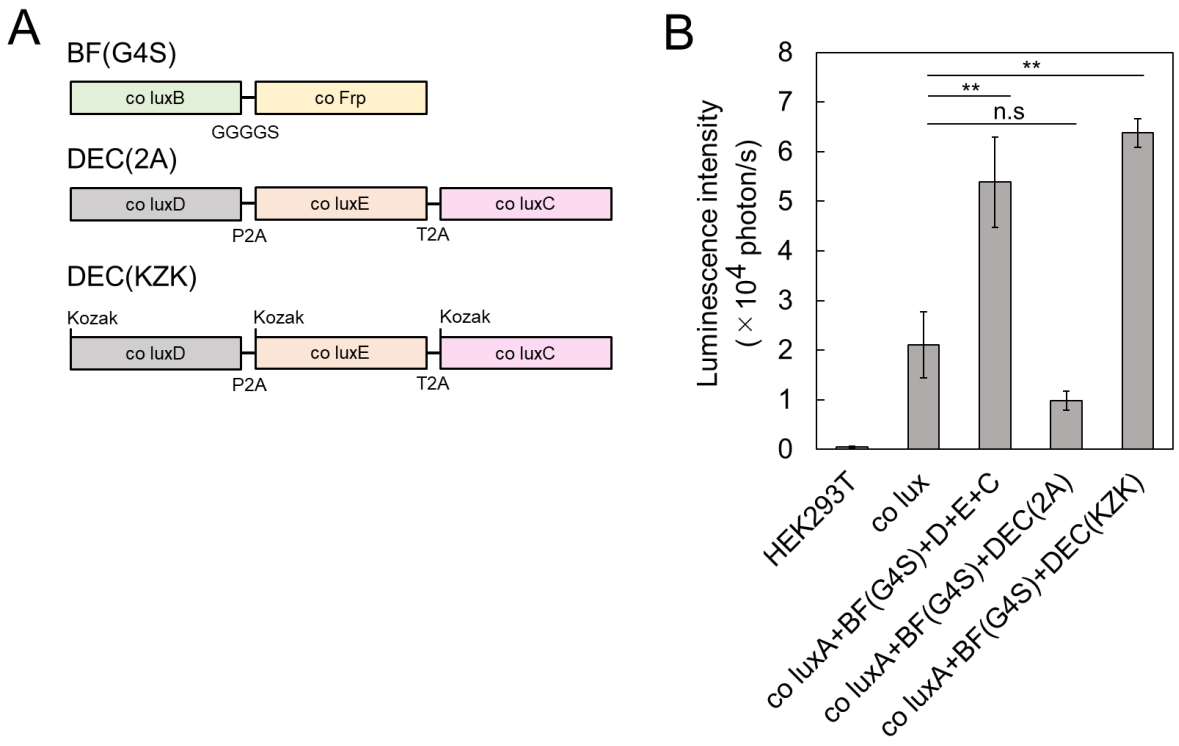

Figure 17. Optimization of co Lux plasmids. (A) Schematics of the optimization co lux plasmids in pcDNA3.1(+) vector. **(B)** Total luminescence intensity of HEK293T cells only, HEK293T cells expressing of co lux plasmids (six plasmid co-transfected), five plasmids co-transfected by fusing co luxB with co Frp using GGGGS (G4S) linker, three plasmids transfected with co luxA, co luxBFrp, and co luxDEC (co luxD-P2A-co luxE-T2A-co luxC), and three plasmids transfected with co luxA, co luxBFrp, and co luxDEC with the addition of Kozak sequence in the downstream of 2A peptide. $n = 3$, $^{**}p < 0.05$.

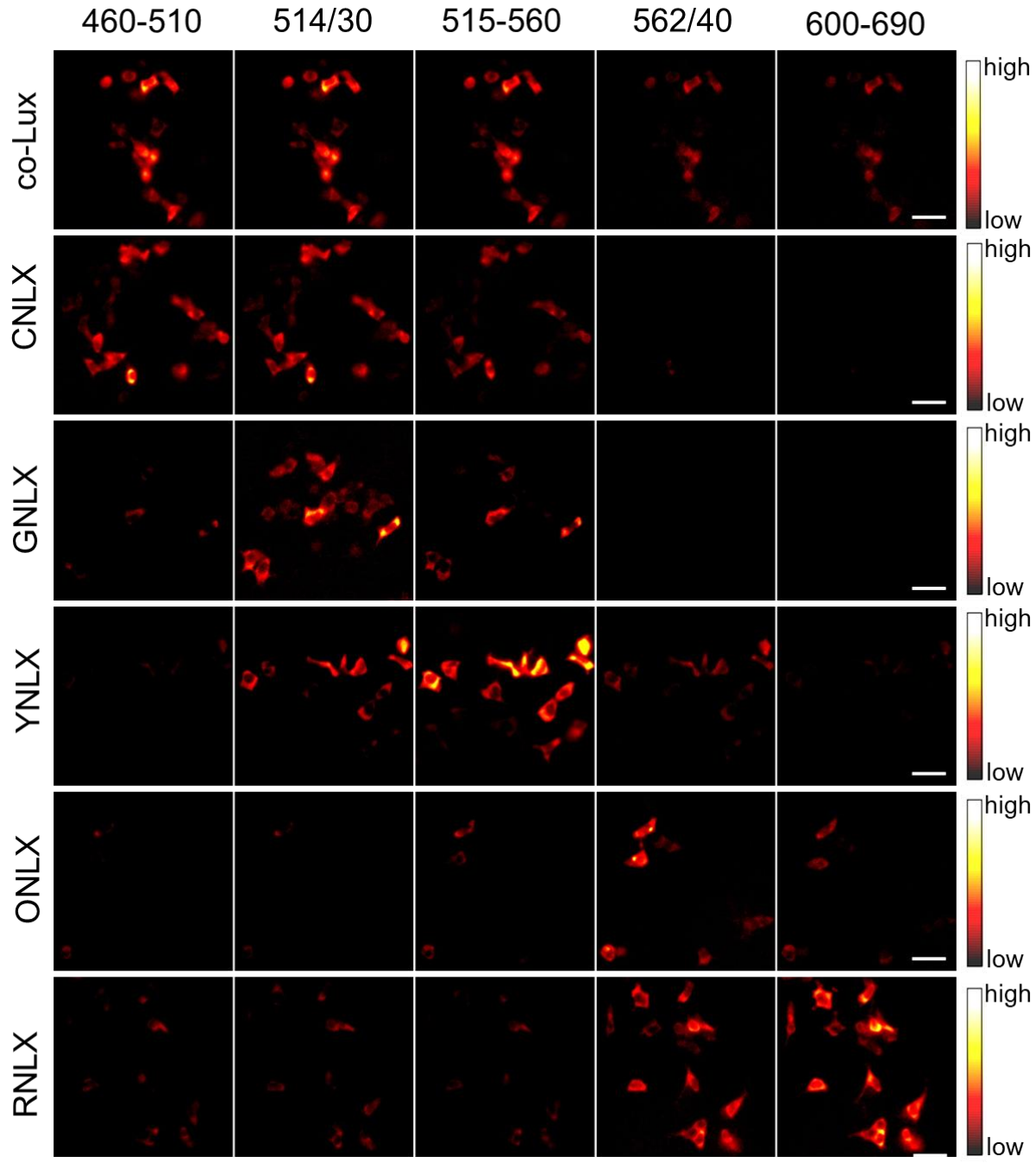

Figure 18. **Auto-bioluminescence imaging of live HEK293T cells expressing NLXs using different optical filters**. Scale bars, 50 µm: ×40 magnification.

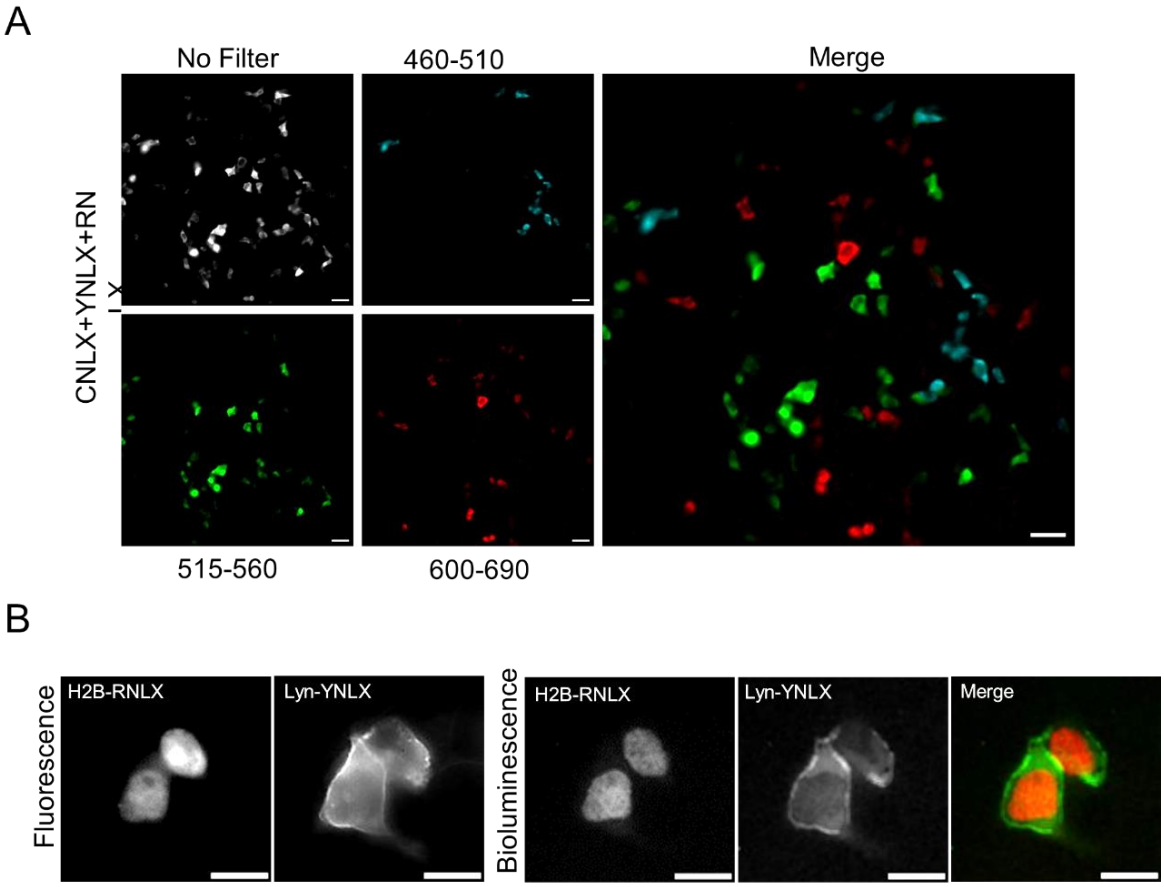

Figure 19. **Multiplexed imaging of live HEK293T cells expressing NLXs. (A)** Auto-bioluminescence imaging of mixed HEK293T cells expressing CNLX, YNLX, or RNLX. Scale bars, 50 µm: ×40 magnification. **(B)** Subcellular tags using NLXs. Bioluminescence imaging of HEK293T cells expressing NLXs targeted to the nucleus (H2B-RNLX) and plasma membrane (Lyn-YNLX). Scale bars, 20 µm: ×100 magnification.

2.3.5 Auto-bioluminescence imaging of NLXs in live *Nicotiana benthamiana* leaves

I discovered that these optimized constructs could be transiently expressed in plant hosts without being optimized for plant codon usage. As a result of introducing the co lux operon constructs into the leaves of *Nicotiana benthamiana*, auto-bioluminescence from the leaves was successfully detected (**Figure 20 and Figure 21A**). NLXs also produced luminescence intensities comparable to those produced by fungal luciferase (nnLuz)[14] (**Figure 21B**). No significant differences I observed in the gene expression levels of NLXs and nnLuz (**Figure 22**). Compared to nnLuz, which generates a single color, NLXs are capable of producing multicolor auto-bioluminescence and serve as versatile reporter genes for plant research. Thus, the NLX-based Lux operon is capable of demonstrating multiplex auto-bioluminescence observations in various living organisms.

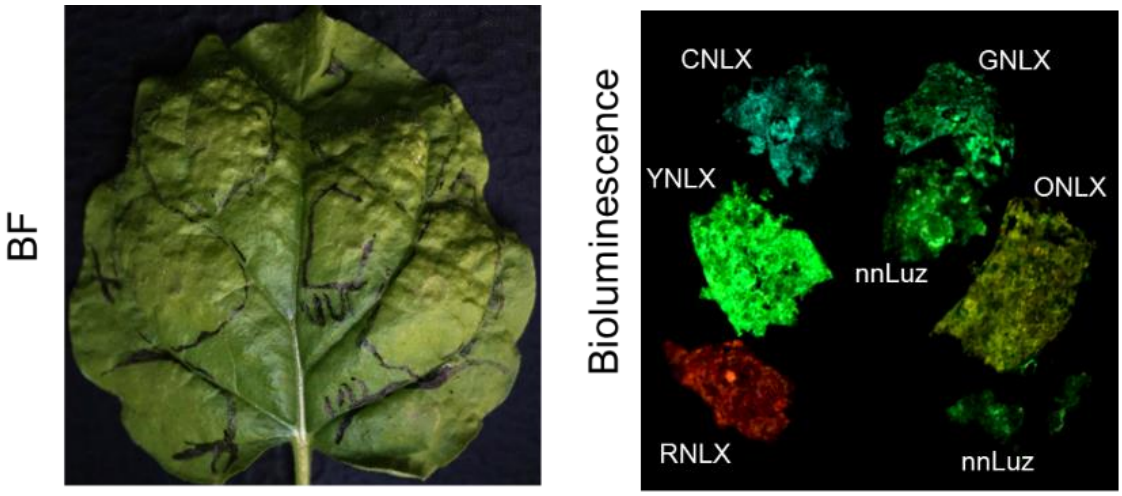

Figure 20. **Multiplexed imaging of live *N. benthamiana* leaves expressing NLXs.** Auto-bioluminescence of *N. benthamiana* leaves expressing NLXs genes and nnLuz. Bioluminescence images were acquired using a Sony α7s camera.

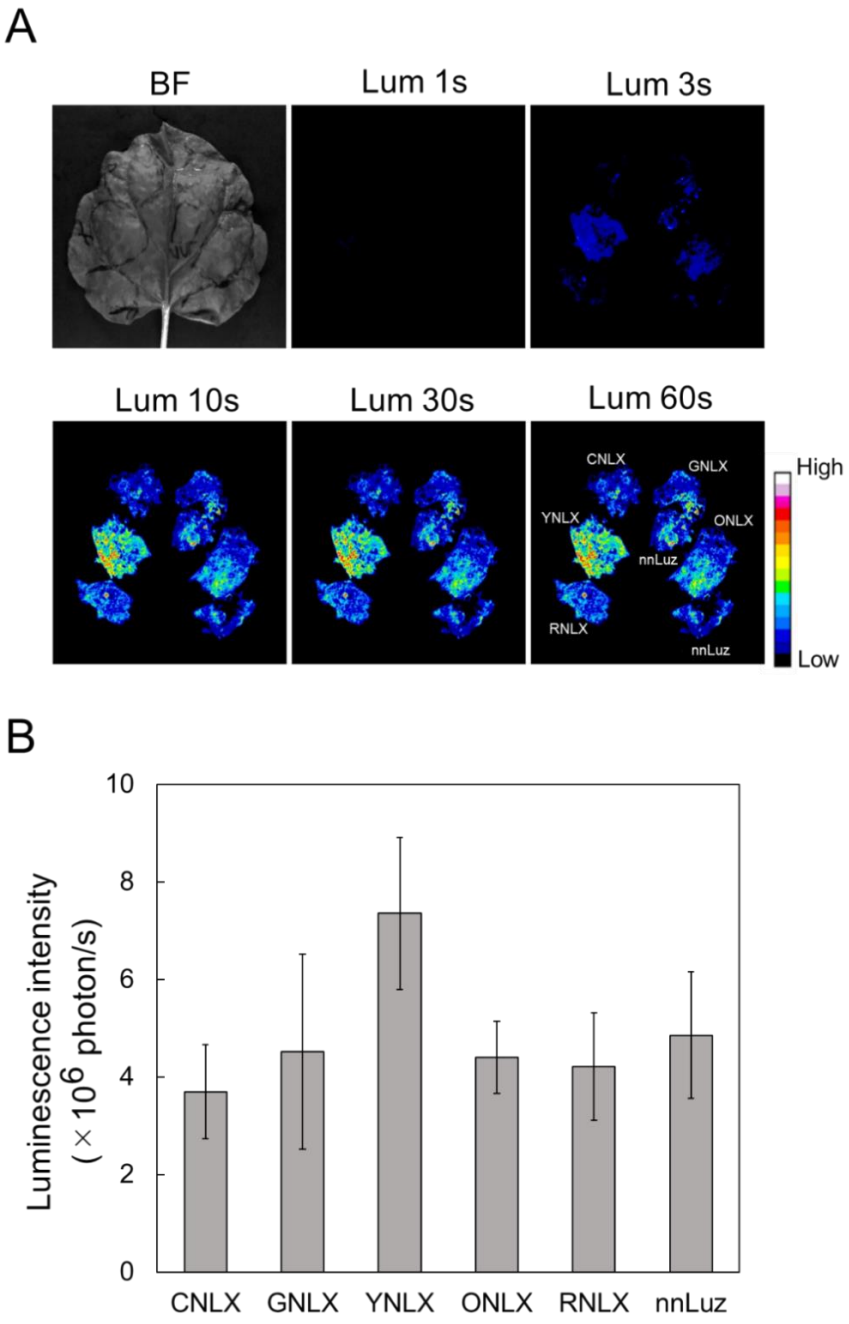

Figure 21. **Auto-bioluminescence of *N. benthamiana* leaves expressing NLXs and nnLuz genes using a CCD-based camera.** Auto-bioluminescence image (**A**) and total luminescence intensity (**B**) of the leaves expressing NLXs and nnLuz variants by *Agrobacterium* infiltration. Luminescence images were taken by CCD camera at several exposure times. Data were measured in triplicate and are presented as luminescence intensities.

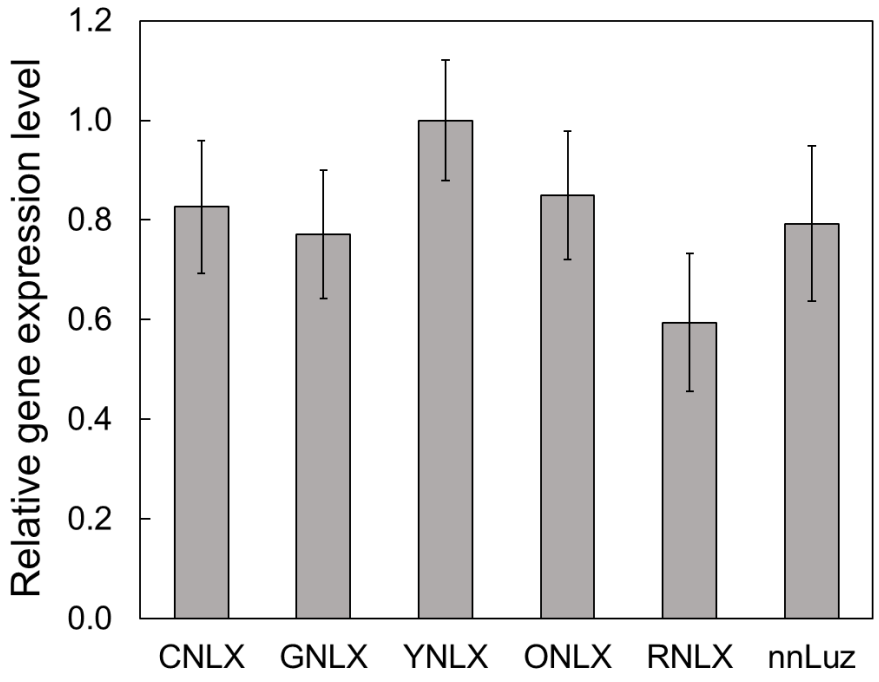

Figure 22. **Relative gene expression levels of NLXs and nnLuz.** The results were normalized to *PP2A* gene expression.

2.4 Conclusion

Here, I successfully developed the first multicolor auto-bioluminescent based on bacterial luciferase, denoted as Nano-lanternX. Through optimization of the LuxA position and BRET donor pairs, I successfully developed five color variants of auto-bioluminescence based on Lux luciferase. These color variants not only shifted the emission spectrum but also increased the luminescence intensity compared to that of wild-type Lux. The cyan version, CNLX, is a brighter variant, potentially up to ten times brighter than wild-type Lux, attributed to changes in quantum yield influenced by the BRET phenomenon. However, the catalytic activity did not change, and there was no significant difference in the k_{cat} values. In addition, to show auto-bioluminescence activity, NLXs genes were transformed into bacterial, mammalian, and plant hosts. I successfully generated multicolor auto-bioluminescent of *E. coli*, HEK293T cells, and *N. benthamiana* leaves. In comparison, the fungi luciferase (Luz) system is only capable of fully establishing auto-bioluminescence in plant hosts and not in other hosts, such as mammalian cells, because of the inability to synthesize caffeic acid as a luciferin precursor in their basal metabolic pathway[7]. Additionally, the NLXs system contradicts the conventional belief that Lux causes low light intensity in the plant host[57]. In fact, my findings revealed that I was able to grow transiently multicolored bright plants with light intensity comparable to that of Luz. Therefore, the NLXs system is an ideal tool for plant research. Overall, NLXs could be a novel tool for tracking novel biological phenomena in real-time observation.

CHAPTER 3

EXPANDING THE APPLICATION OF NLXs

3.1 Introduction

The application of bacterial luciferase as a biosensor has been limited to a single reporter[8-11]. Another application is its auto-bioluminescent pathway, which also uses energy (ATP and NADPH) to produce luciferin and $FMNH_2$. As a result, a specific molecule that can inhibit energy metabolism decreases luciferin production, thus lowering luminescence intensity. However, the response is not sensitive to direct energy production and requires a longer time (approximately an hour)[34]. Therefore, it is necessary to expand the application of Lux as an auto-bioluminescent probe for multiplexed applications in biosciences.

Lux systems are also promising for high-throughput screening (HTS) and cost-effective owing to the diminishing addition of luciferin. However, a recent Lux system still uses another luciferase to normalize luminescence intensity because of the imbalance in transfection efficiency. Therefore, a single Lux color is not suitable for multiple reporters. Here, I aimed to expand the application of bacterial luciferase using NLXs to evaluate multiple reporter assays and protein-based sensor development. I demonstrated the proof-of-concept of a dual reporter assay using YNLX and RNLX as HTS markers to evaluate the effect of agonist compounds on Wnt-responsive gene expression.

The Wnt signaling pathway, also known as the Wnt/β-catenin pathway, includes β-catenin accumulation and translocation into the nucleus, which activates target genes under-or via T-cell factor/lymphoid enhancer-binding factor (TCF/LEF) transcription factors[58,59]

(**Figure 23**). Once activated, it facilitates the expression of the genes involved in cell proliferation, survival, differentiation, and migration[60].

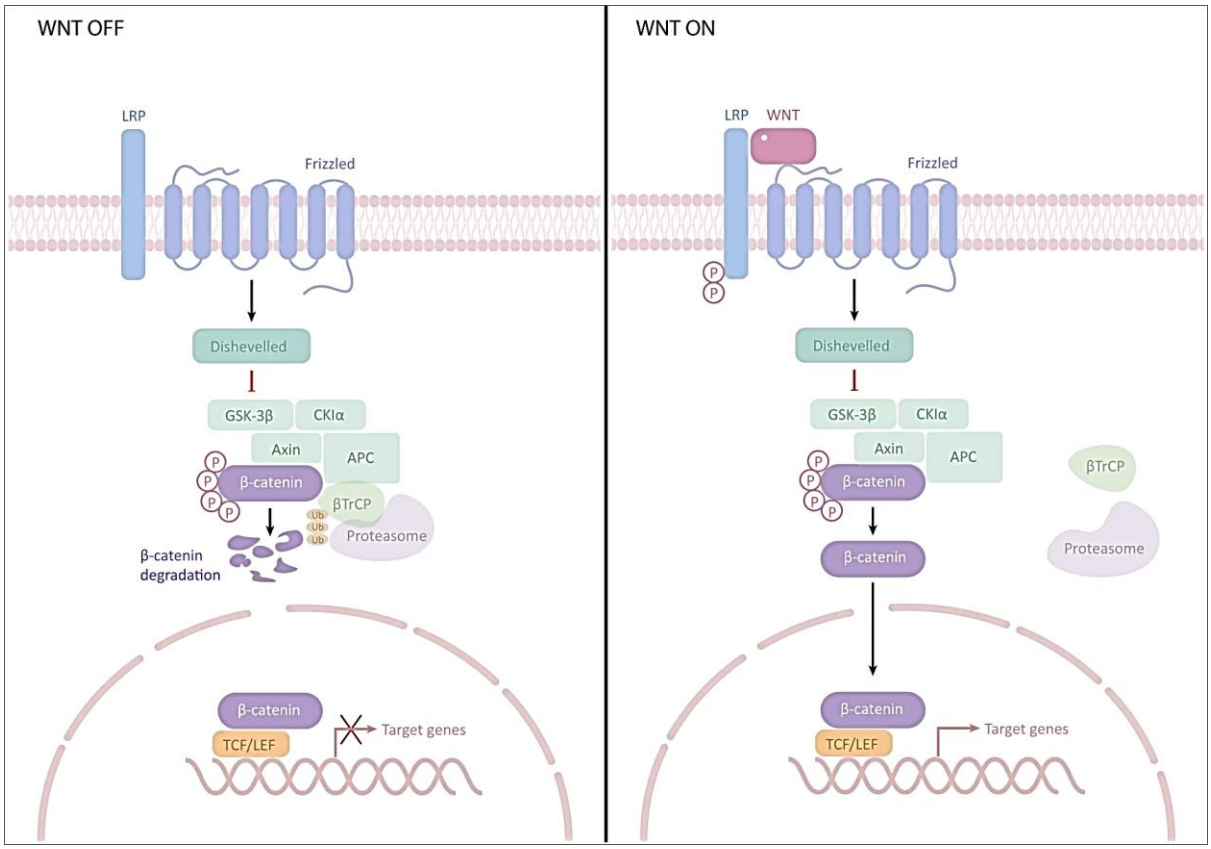

Figure 23. **Schematic representation of the Wnt/β-catenin signalling pathway.** Adopted from Liu, *et al*[59]. The left panel shows the inactivation of Wnt signalling. In the absence of Wnt ligands, β-catenin is degraded by forming a complex with glycogen synthase kinase 3β (GSK-3β), Axin, adenomatous polyposis coli (APC), CK1α, and E3 ubiquitin ligase β-trcp. The right panel shows activation of Wnt signalling. In the presence of Wnt ligands that bind to the receptor, Axin binds to phosphorylated lipoprotein receptor-related protein (LRP), resulting in disruption of the β-catenin complex. β-catenin migrates to the nucleus, binds to TCF, and activates the expression of its downstream target genes.

Bioluminescence has not only been utilized for detecting gene expression in response to specific promoters but has also been employed in various biosensor applications by attaching luciferase to bioactive proteins. There are two types of luciferase-based biosensors, first is uses split-luciferase strategy[61], which one parts of the luciferase molecule is split with the sensor domain, and the other part is fused with the peptide that binds to the sensor domain. As a result, in the presence of bioactive molecules, the split luciferase forms a complex as a functional luciferase and emits luminescence. The other uses a ratiometric strategy, using a BRET-based indicator[62] that comprises the bioactive protein inside the fusion of luciferase and fluorescent protein as a donor and acceptor, respectively. In this strategy, the signal from the bioactive molecules represents a change in the BRET signal. Both biosensor types are non-auto-bioluminescent, which is substrate-dependent luciferase, resulting in a luminescence signal decrease over time. However, no auto-bioluminescent protein-based biosensors have been developed to date. Thus, I developed a protein-based sensor of active molecules, such as calcium and ATP, for evaluation in *in vitro* and live HEK293T cells. To the best of my knowledge, this is the first report on the development of calcium and ATP sensors based on auto-bioluminescence, especially in bacterial luciferase.

.

3.2 Materials and methods

Gene construction. I construct the Wnt-responsive enhancer 7× TCF and minimal CMV promoter by PCR-amplified from pT2-7×TCF-NLS-YNL[31] and subcloned into pcDNA3.1(+)-YNLX to obtain pcDNA3.1(+)-7×TCF-minCMV-YNLX. For Ca^{2+} indicators, I PCR-amplified the Troponin C (TnC)[63] from pRSET$_B$-Twitch-2B and subcloned it into the N-terminus of LuxA in pRSET$_B$-YNLX. I constructed a series of BRET-based Ca^{2+} indicators by replacing VenusΔC10 in pRSET$_B$-YNLX with circularly permutated Venus (cp173Venus-TnC-LuxA) variants from yellow cameleon (YCs) variants. I next subcloned the cp173Venus-TnC-LuxA into pcDNA3.1(+)-YNLX vector for mammalian expression. For the ATP indicator, I PCR-amplified ε subunit[64] from pRSET$_B$-AT1.03, subcloned it into the N-terminus of LuxA of pRSET$_B$-YNLX, and pcDNA3.1(+)-YNLX for bacterial and mammalian expression, respectively. All constructs were subcloned using the TEDA method.

Protein purification. I transformed *E. coli* strain JM109(DE3) (Promega) with the pRSET$_B$ plasmid harboring NLXs variants fused with an N-terminal polyhistidine tag by heat shock method at 42 °C for 45 s. I spread the transformants on an LB plate containing 100 μg/mL carbenicillin and incubated at 37 °C for overnight. I grew *E. coli* in a 200 mL LB medium containing 100 μg/mL carbenicillin at 23 °C for 60 h with gentle shaking at 120 rpm. I collected the *E. coli* cells by centrifugation, suspended them in phosphate buffered saline solution (PBS; Takara Bio) and ruptured using a French press (ThermoFisher Scientific). I purified the supernatant using Ni-NTA agarose affinity columns (Qiagen), washed it with 10 mM imidazole (FUJIFILM Wako) and eluted with 100 mM imidazole. Finally, I changed the buffer elution to 20 mM HEPES (pH 7.4) using a PD-10 column (GE Healthcare), quickly froze the protein solution in liquid nitrogen, and stored them at −80 °C.

Characterization of Ca^{2+} indicators based on NLXs. I measured the emission spectra of the purified Ca^{2+} indicator based on Lux and its variants by using PMA-12 (Hamamatsu Photonics) with 20 s exposure. I used the final protein concentration by 8 μM and then mixed with 10 μM FMN, 20 μM decanal, and 100 μM BNAH. I performed Ca^{2+} titrations by the reciprocal dilution of Ca^{2+}-free and Ca^{2+}-saturated buffers containing 10 mM MOPS, 100 mM KCl, and 10 mM EGTA with or without 10 mM Ca^{2+} added as $CaCO_3$, at pH 7.2, 25 °C. Then, I calculated the free Ca^{2+} concentrations using 0.15 mM as the apparent K_d value of EGTA for Ca^{2+}. I used the Ca^{2+} titration curve to calculate the apparent K_d value using nonlinear regression analysis. I fitted the averaged to a single Hill equation using Origin8 software (OriginLab) for final results.

Characterization of ATP Indicator based on NLXs. I measured the emission spectra of the purified ATP indicator based on Lux at 25 ˚C in HEPES using a microplate reader (SH-9000, Corona Electric) with 1s exposures. I used the final protein concentration by 8 μM and then mixed with 10 μM FMN, 20 μM decanal, and 100 μM BNAH. I mixed the final ATP solution (10 mM) with equimolar $MgCl_2$ to obtain the MgATP complex.

Mammalian cell culture and transfection. I cultured HEK293T cells in Dulbecco's Modified Eagle's Medium (DMEM) (Sigma-Aldrich) supplemented with 10% fetal bovine serum (FBS; Biowest) at 37 °C in 5% CO_2. I seeded cells on collagen-coated 35 mm glass-bottom dishes or 12-well dishes. For transfection, I transfected the recombinant DNA using polyethylene imine (PEI Max 40 K; Polyscience), according to the manufacturer's instructions. The final concentration of all plasmids transfected was one μg/mL. I cultured the cells for ~48 h and

exchanged the medium with phenol red−free DMEM/F12 (ThermoFisher Scientific) and used it for imaging or assay.

Bioluminescence imaging. l performed microscopy luminescence imaging with an inverted microscope based on the IXplore^{TM} Live system equipped with an EM-CCD camera (Andor iXon Ultra 888). For the Wnt reporter, I used an Olympus U-FYFP filter with 2 min of exposure, EM-gain of 1000x, x20 objective lens, and 2 × 2 binning settings. For YNLX(Ca^{2+}), I used Olympus U-FCFP and Olympus U-FYFP filters with 2 min of exposure, EM-gain of 1000×, ×40 objective lens, and 2 × 2 binning settings with or without the addition of 10 mM ionomycin and 10 mM $CaCl_2$. For YNLX(ATP), I used Olympus U-FCFP and Olympus U-FYFP filters with 3 min of exposure, EM-gain of 1000×, ×40 objective lens, and 2 × 2 binning settings with or without the addition of ATP inhibitors (20 μg/mL oligomycin A and 20 mM 2-deoxyglucose). I performed all imaging conditions at 37 °C, 5% CO_2 environment in a stage-top incubator, STX (TOKAI HIT). All bioluminescent images were analyzed using ImageJ software[65] and MetaMorph software.

Luciferase assay. For the luciferase assay of the Wnt reporter, I transfected the original co lux, 7×TCF-minCMV-YNLX with or without co-transfected with CMV-RNLX plasmids into HEK293T cells in 12 well dishes. After 12 h of transfection, I treated the cells with or without LiCl for 16 h. Then, I transferred the cells to a 96-well white microplate and measured the luminescence using a multimode plate reader (Spectra Max iD5, Molecular Devices) for 1 s of exposure. I used the luminescence intensities at 530 nm (YNLX signal) and 590 nm (RNLX signal) emission spectra to determine the effect of various LiCl concentrations. The reported

unit was the luminescence intensity (RLU) of the 530 nm signal over the 590 nm signal. To derive the fold of activation, I normalized all values to the corresponding non-treated control.

Data analysis and statistical methods. All bioluminescent images from the microscope were analyzed using ImageJ and MetaMorph software. I used the pseudocolor images for microscopy images with "Red Hot" color for total luminescence intensity and a specific color for each cell according to specific wavelengths. To produce ratio images of the Ca^{2+} and ATP sensors, I processed the ratio images with MetaMorph, and used pseudocolor to distinguish the ratio values.

I performed data fitting and statistical analysis using Origin8 (OriginLab). I performed statistical analysis using unpaired Student's t-test for comparing two parameter sets, and I used one-way ANOVA followed by post hoc Tukey's honestly significant difference test to compare more data sets.

3.3 Results and discussion

3.3.1 Application of NLXs as gene expression

Luciferase-based probes such as *Renilla* luciferase (Rluc) and firefly luciferase (Fluc)[66] have been widely used as reporter genes. However, luciferase-based probes still rely on luciferin addition. Thus, the ability to monitor the dynamics of reporter genes at the single-cell level for long-term observation without a decrease in luminescence intensity is limited. To evaluate whether our NLXs can also be used in reporter gene assays, I carried out a Wnt-reporter assay utilizing the Wnt-responsive promoter 7×TCF[31]. The addition of LiCl as an agonist chemical to the Wnt protein resulted in luminescence from the cell-encoded 7×TCF-YNLX plasmid (**Figure 24A**). I also checked whether the addition of LiCl or Wnt-activation can affect the luminescence intensity of cells expressing Lux systems (co lux). No significant changes in auto-bioluminescence intensity I observed after the addition of LiCl compared to cells expressing the Wnt-responsive promoter 7×TCF (7×TCF-YNLX) (**Figure 24B**).

To track the dynamics of Wnt responsiveness at the single-cell level, I continued to express 7×TCF-YNLX in HEK293T cells for 16 h. I observed the bioluminescence for four hours into the observation period (**Figure 25A**) and continued to be expressed (**Figure 25B**). Thus, the reporter gene based on YNLX was successfully used to monitor the dynamics of the reporter gene for long-term imaging. I next demonstrated this reporter's utility in transient transfection for high-throughput screening (HTS) by co-transfecting CMV-RNLX and 7×TCF-minCMV-YNLX in HEK293T cells, producing normalized data accounting for varying transfection efficiencies (**Figure 26A-B**). Unlike previous reporter assays utilizing Lux[67], which relied on Fluc or Rluc to normalize luminescence intensity and required cell lysis in downstream processes, the NLX system eliminates the need for additional luciferases and the

requirement for cell lysis. This feature enhances convenience and cost-effectiveness, making it particularly advantageous for HTS applications.

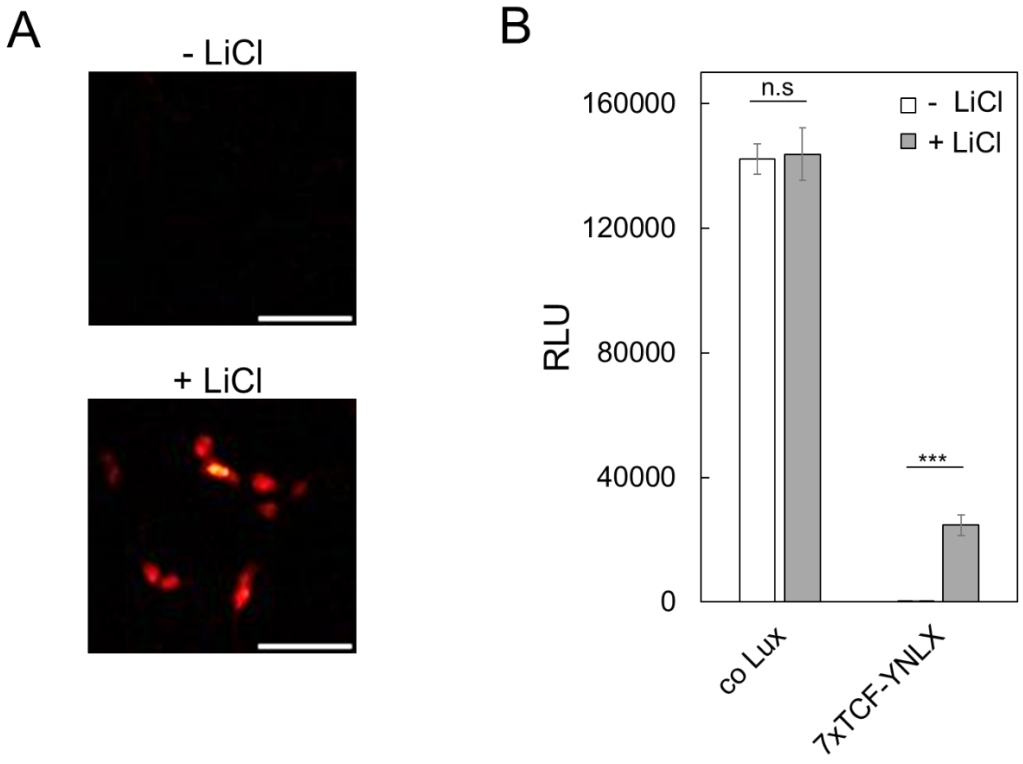

Figure 24. Reporter assay for Wnt gene expression by YNLX. Auto-bioluminescence imaging **(A)** and auto-bioluminescence intensity **(B)** of HEK293T cells expressing co lux and 7×TCF-YNLX were measured at 16h with or without the addition of 40 mM LiCl. Scale bars, 100 μm: ×20 magnification. RLU is the relative light unit. Data are mean ± s.d. $n = 3$, *** $p < 0.001$.

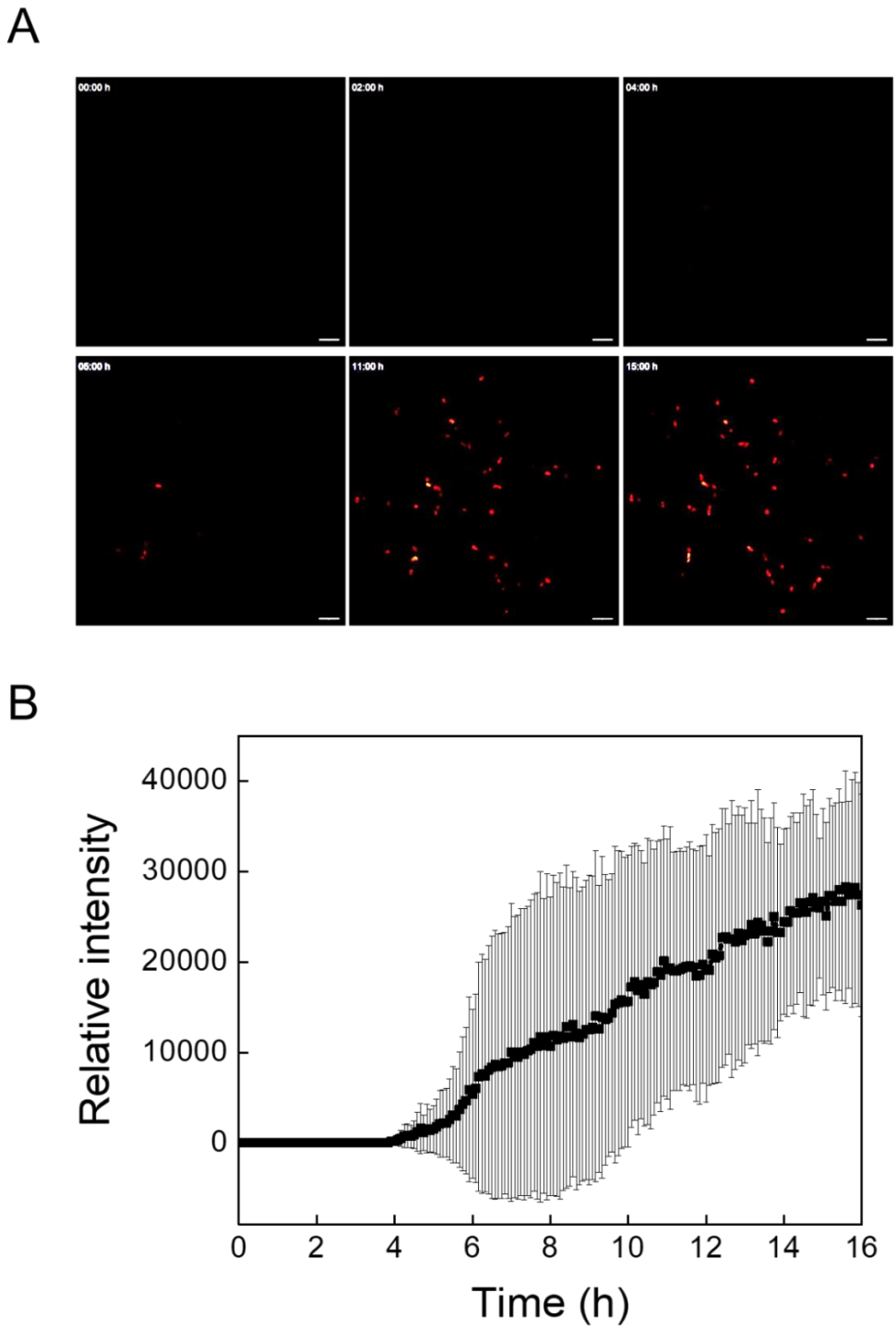

Figure 25. Reporter time-lapse imaging of 7×TCF-YNLX. Sequential images (A) and time courses (B) of HEK293T cells expressing 7×TCF-YNLX upon the addition of 40 mM LiCl. Scale bars, 100 μm: ×20 magnification

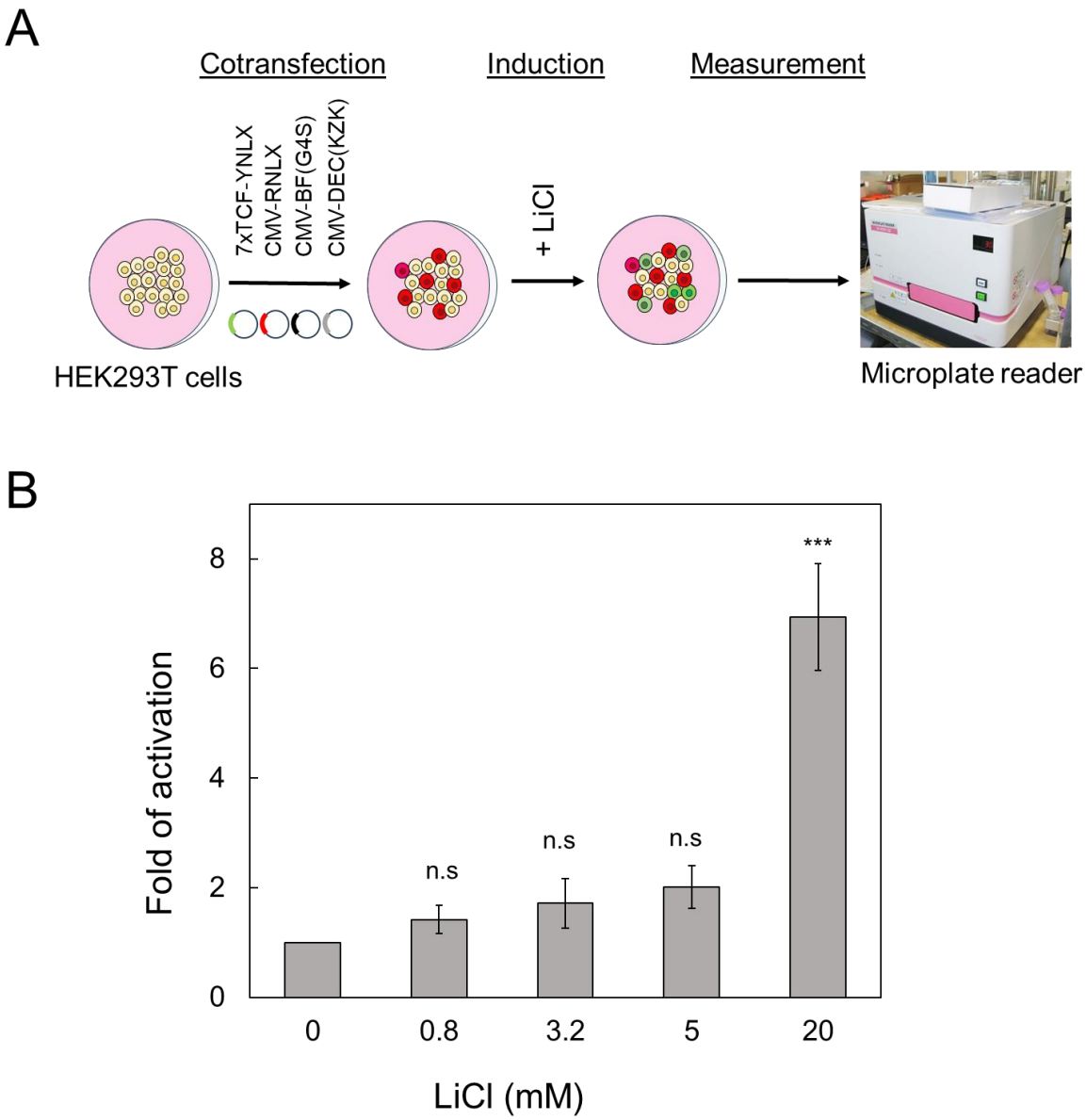

Figure 26. Multiplex assay with NLXs. (A) Schematic of the multiplex assay. HEK293T cells transiently transfected with 7×TCF-YNLX, CMV-RNLX, and auto-bioluminescent parts (CMV-BF(G4S) and CMV-DEC(KZK)) plasmids were treated with LiCl to induce Wnt expression. **(B)** Auto-bioluminescence intensities of 7×TCF-YNLX upon the addition of various concentrations of LiCl. The bioluminescence intensities were measured 16 h after the addition of various concentrations of LiCl. Data are mean ± s.d. $n = 3$, ***$p < 0.001$.

3.3.2 Application of NLXs as protein-based indicator for ion

I expanded the application of Lux luciferase by developing a novel protein-based indicator for ion detection, such as calcium. I first developed split-indicator strategy of calcium indicator based on YNLX (**Figure 27A**). This strategy led to an increase in the luminescence intensity in the presence of calcium. I selected a flexible residue in the LuxA or LuxB. I found that, according to the crystal structure (PDB: 3FGC), the non-structural K283/G284 of LuxA and G166/G167 of LuxB are far away from the active site of LuxA and the interaction site of LuxA with LuxB (**Figure 27B**). However, the luminescence intensity of these constructs was lower (only 3%) than that of the original YNLX, although it showed the highest signal change, 258% for YNLX-CaM-A(283/284) and 197% for YNLX-CaM-B(166/167) in the presence of calcium (**Figure 29**).

Next, I employed a ratiometric indicator strategy (**Figure 28**). I fused the Ca^{2+}-sensitive troponin-C peptide (TnC)[63] into the site between Venus and LuxA in the YNLX plasmid. In comparison with the split-indicator strategy, the ratiometric indicator strategy did not show a decrease in luminescence intensity and showed a signal change (90%) upon the addition of calcium, although the signal change was not higher than that of the split-type YNLX-CaM variants (**Figure 29**). Therefore, I used a ratiometric strategy to develop a calcium indicator based on YNLX.

I screened Venus variants and circularly permutated Venus variants[68] to achieve the highest dynamic range upon Ca^{2+} addition (**Figure 30**). Among them, I found that cp173Venus-TnC-LuxA (YNLX(Ca^{2+})) showed the highest dynamic range (181%) compared with the other variants (**Figure 31A**). In addition, the cpVenus variant fusion, except cp173Venus, showed the lowest luminescent signal for an unknown reason (even though the fluorescence of the Venus moiety was not changed). I speculated that this was similar to the optimization of Venus

in the N- or C-terminus of LuxA (**Figure 8),** which could be the disruption of protein folding of LuxA, especially in the formation of the TIM β/α barrel structures of LuxA.

The K_d value for Ca^{2+} in this construct was 570 nM and the Hill coefficient was 1.02 (**Figure 31B**). Compared to other calcium sensors, the dynamic range of YNLX(Ca^{2+}) is relatively low. It showed a comparable K_d value for Ca^{2+} compared to other non-auto-luminescent, such as GeNL(Ca^{2+})_480[32], Nano-lantern (Ca^{2+})[30] or CalvluxVTN[69] (**Table 5**). The K_d of YNLX(Ca^{2+}) was higher and exhibit lower dynamic range compared with ratiometric-based Ca^{2+} indicator of fluorescent protein, such as YC3.60[68] and Twitch-2B[63]. However, the dynamic range and K_d value of YNLX (Ca^{2+}) were better than those of previous ratiometric Ca^{2+} indicators of Rluc8 such as BRAC[62] (**Table 5**).

To determine whether the YNLX(Ca^{2+}) sensor could be used *in cellulo,* I transiently expressed YNLX(Ca^{2+}) in cultured cells under the control of the CMV promoter. I successfully observed the calcium changes before and after the addition of ionomycin and 10 mM $CaCl_2$ (**Figure 31C**). Luminescence was representative of the BRET ratio of YNLX(Ca^{2+}) in the presence of 10 mM $CaCl_2$. Compared with previous ratiometric Ca^{2+} indicators such as BRAC or CalvluxVTN, YNLX(Ca^{2+}) is suitable for producing BRET ratio signals without the addition of luciferin. Thus, YNLX(Ca^{2+}) is promising for the long-term observation of calcium dynamics *in cellulo*.

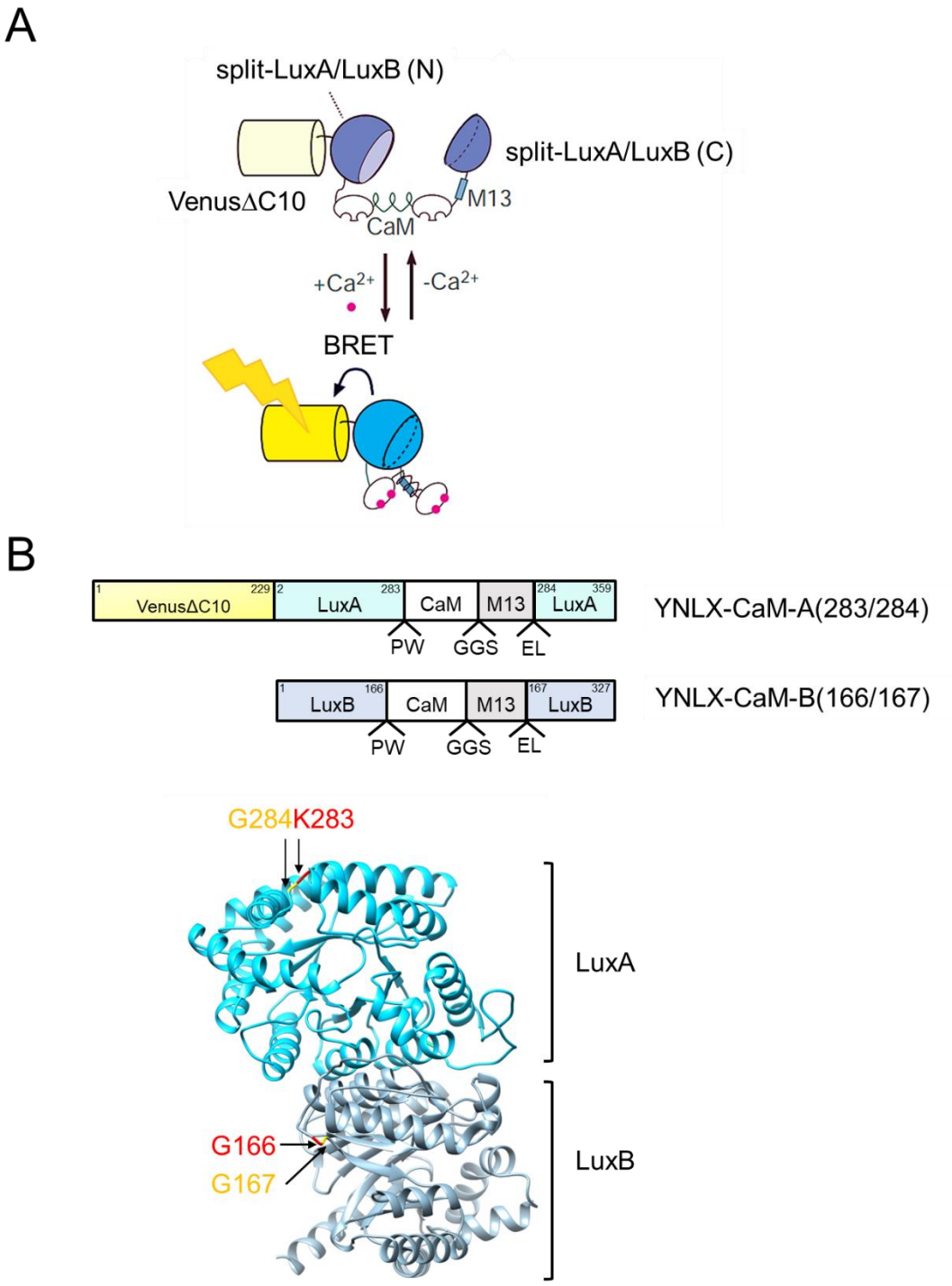

Figure 27. Schematic of split-YNLX for the calcium biosensor. Schematic images of split-YNLX (A) and schematic constructs and three-dimensional structure of Lux (PDB: 3FGC) with the position of the insertions (LuxA-283/284 and LuxB-166/167)

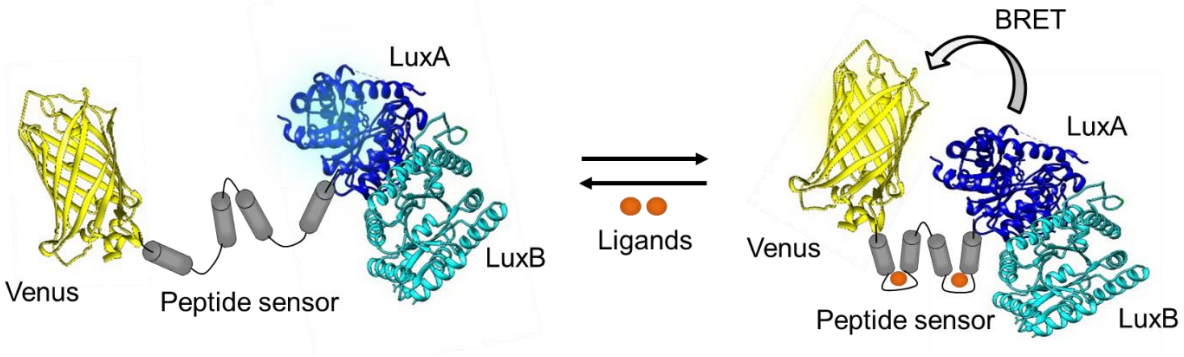

Figure 28. Schematic of protein-based sensor based on NLXs using a ratiometric strategy.

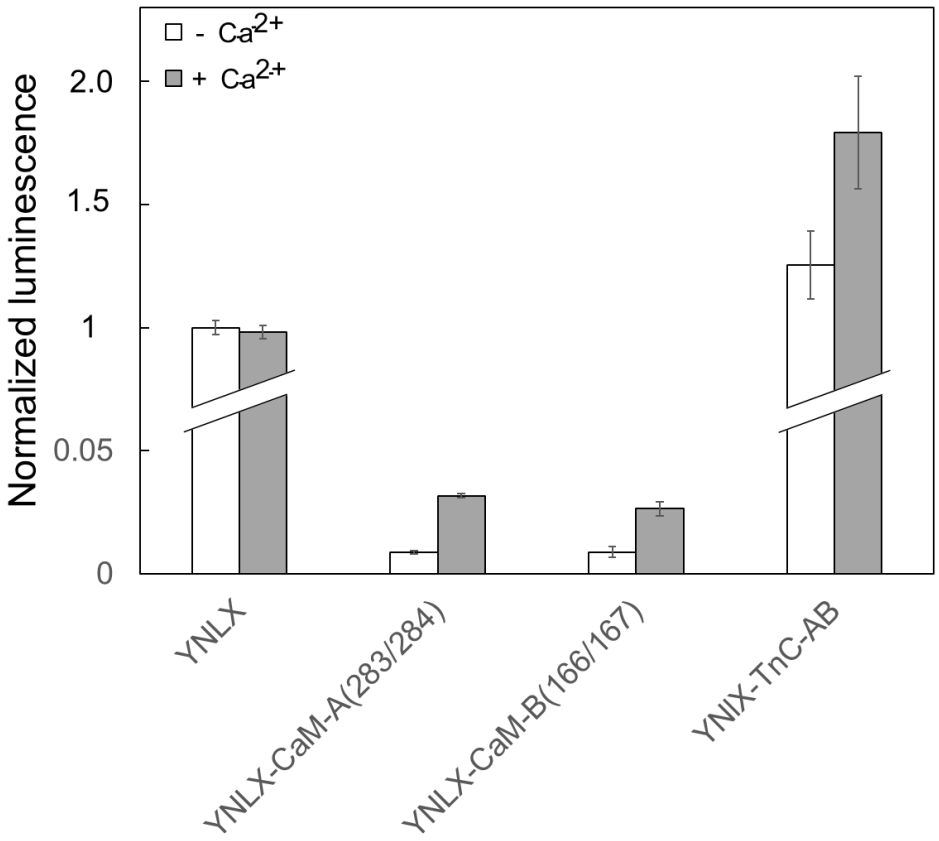

Figure 29. Relative brightness of recombinant YNLX, YNLX-CaM-A(283/284), YNLX-CaM-B(283/284), and YNLX-TnC-AB with or without Ca^{2+}.

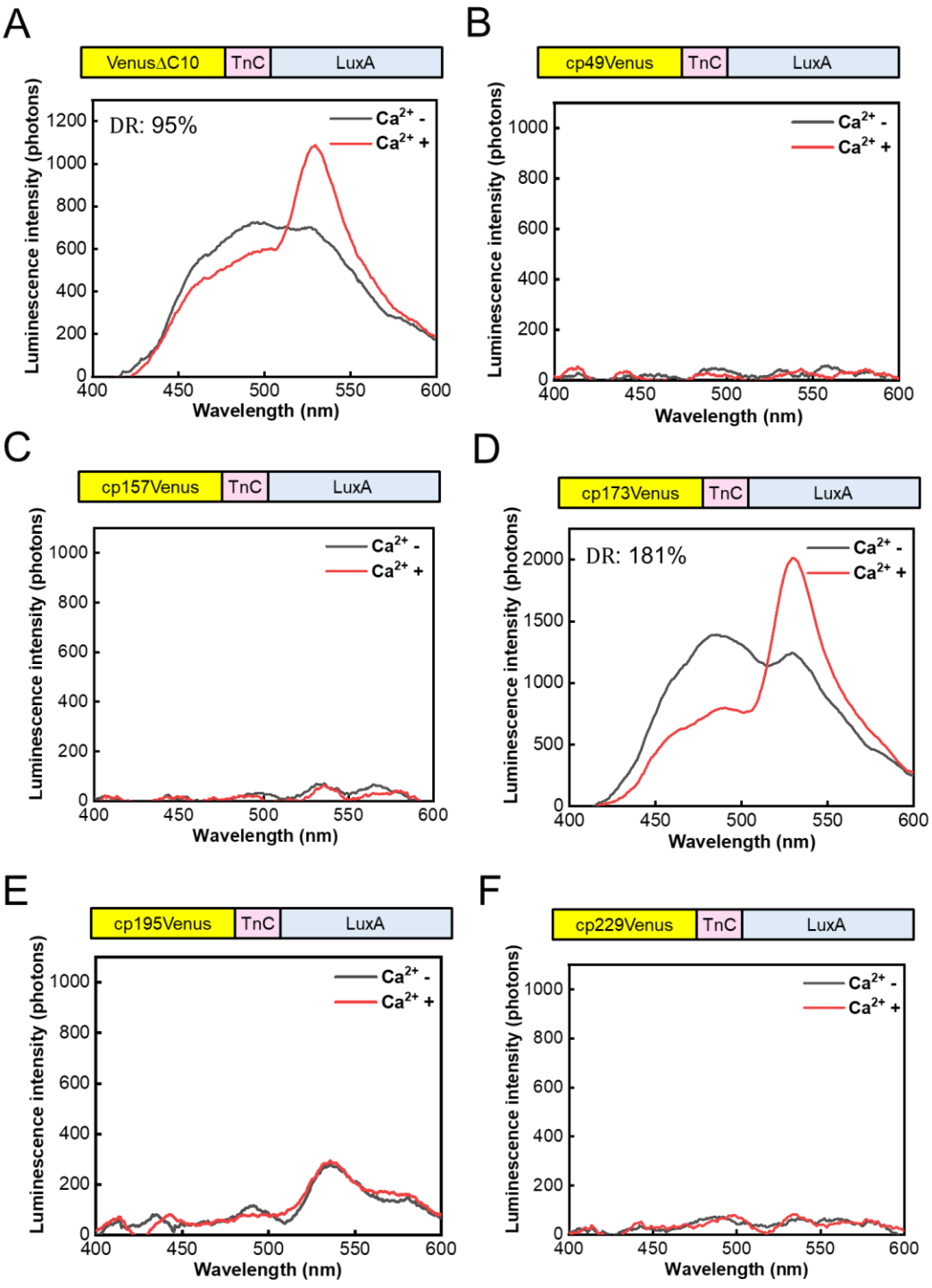

Figure 30. Optimization of calcium indicators based on YNLX. Schematic (upper parts) and emission spectra (lower parts) of the calcium indicator based on NLX, a-f. Venus or cpVenus variants-TnC-LuxA, under 10 mM EGTA (black) and 20 µM $CaCl_2$ (red). Data were measured in triplicate and are presented as luminescence intensities.

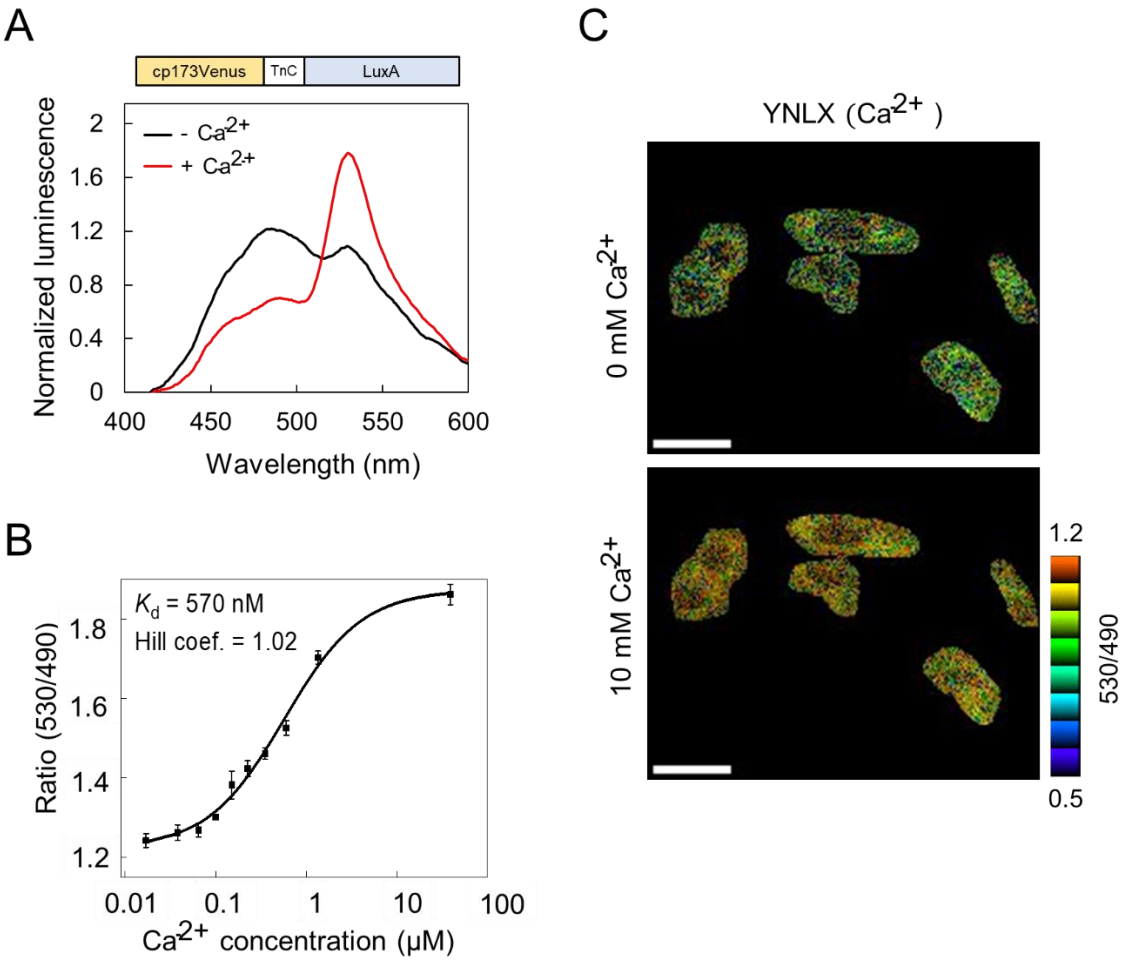

Figure 31. Characterization of YNLX(Ca^{2+}) in *in vitro* and live HEK293T cells. (A) Emission spectra of YNLX(Ca^{2+}) with and without Ca^{2+}. Bioluminescence intensities were normalized by the isoemission point. **(B)** Ca^{2+} titration curve of YNLX(Ca^{2+}). The bioluminescence ratio was calculated from the peaks at 490 and 530 nm. **(C)** Auto-bioluminescence imaging of YNLX(Ca^{2+}). BRET ratio (pseudocolor images) of HEK293T cells expressing YNLX(Ca^{2+}) before and after addition of 10 μM ionomycin and 10 mM $CaCl_2$. Scale bars, 50 μm: ×40 magnification.

Table 5. Affinity for Ca^{2+} of YNLX (Ca^{2+}) and other Ca^{2+} sensor

	Dynamic range (%)	K_d (nM)	Hill coefficient	Biosensor types, donor/acceptor	References
YNLX(Ca^{2+})	181	570	1.02	Auto-LP, Lux/cp173Venus	This study
BRAC	60	1900	1.3	Non auto-LP, Rluc8/Venus	Saito, *et al*[62]
GeNL(Ca^{2+})_480	490	480	1.2	Non auto-LP, split-mNeonGreen	Suzuki, *et al*[32]
Nano-lantern (Ca^{2+})	300	620	1.4	Non auto-LPs, split-YNL	Saito, *et al*[30]
CalfluxVTN	530	480	1.36	Non auto-LP, NLuc/cp173Venus	Yang, *et al*[69]
YC3.60	560	250	2.4	FP, ECFP/cp173Venus	Nagai, *et al*[68]
Twitch-2B	800	200	1.3	FP, mCerulean3/cpVenus^{CD}	Thestrup, *et al*[63]

*Auto-LP (Auto-bioluminescence protein) and FP (Fluorescent protein)

3.3.3 Application of NLXs as protein-based indicator for molecule

I have expanded the application of NLXs as protein-based indicators for important molecules, such as ATP. To develop an ATP indicator based on Lux, I fused the ε subunit[64] into the site between Venus and LuxA in YNLX, resulting in the Venus-ε subunit-LuxA (YNLX(ATP)). Similar to the ATP indicator based on fluorescent proteins, such as ATeam[64], the dynamic range of the BRET ratio was not considerably larger than that of the calcium indicator. It should be noted that the structure of the ε subunit was quite large (14 kDa) compared to that of TroponinC (8 kDa), thus reducing the BRET efficiency.

I found that YNLX(ATP) showed elevated BRET efficiency in the presence of ATP, with the K_d value for ATP of this construct being 2.3 mM (**Figure 32A-B**). YNLX(ATP) was designed as a low-affinity ATP sensor; thus, it is suitable for measuring physiological ATP level (1-5 mM)[70]. YNLX(ATP) also showed a K_d value comparable to that of previous non-auto-bioluminescent ATP indicators that used a ratiometric strategy, such as BTeam[71], or fluorescent type, such as ATeam (**Table 6)**. Therefore, I continued to evaluate the functionality of YNLX(ATP) in mammalian cell experiments.

To check the functionality of this sensor, I transiently expressed YNLX(ATP) in HEK293T cells under the control of the CMV promoter. Because the ATP levels in HEK293T cells were well maintained under good environmental conditions, I used 2-deoxyglucose and oligomycin A were used as inhibitors of glycolysis and oxidative phosphorylation, respectively. I successfully observed the BRET ratio signal upon the addition of these inhibitors (**Figure 32C).** In addition, I confirmed the long-term imaging of YNLX(ATP) after the addition of these inhibitors (**Figure 33).** These results indicate that YNLX was successfully engineered as an ATP indicator to visualize ATP dynamics at the single-cell level.

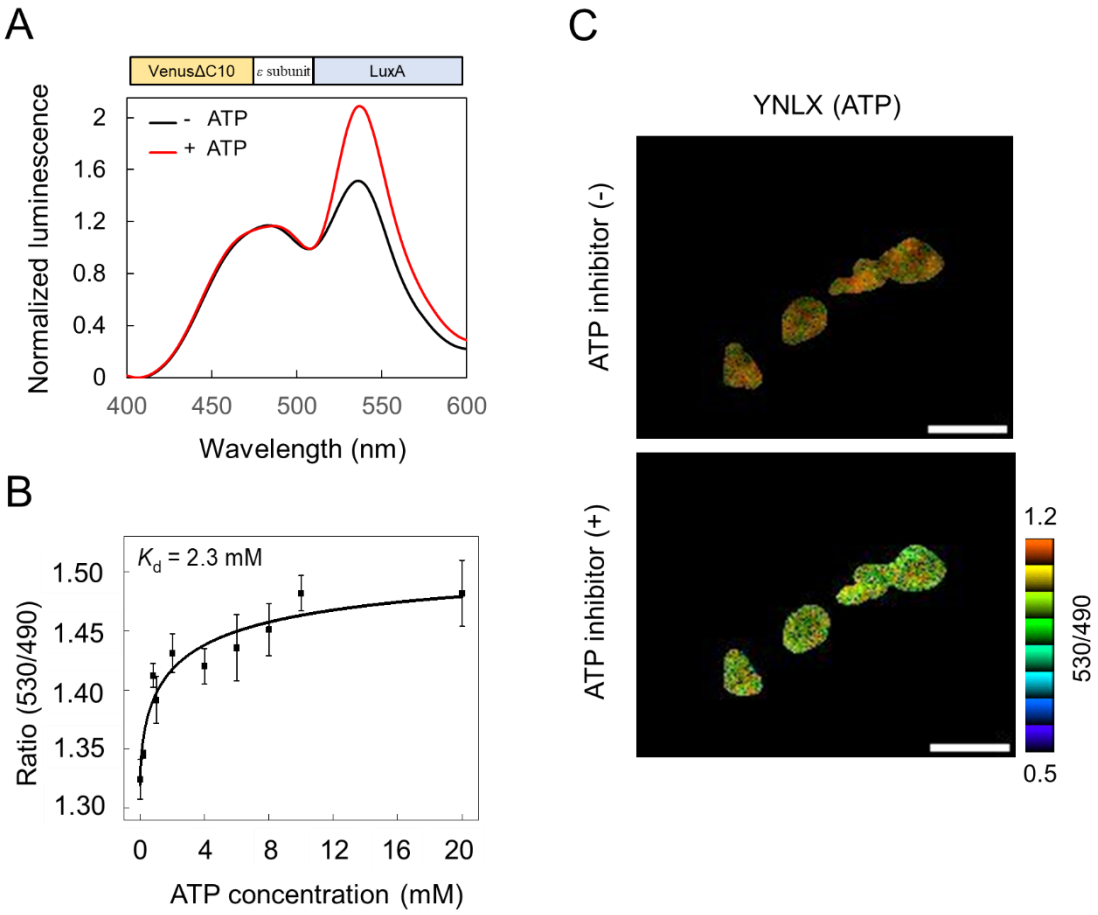

Figure 32. Characterization of YNLX(ATP) in *in vitro* and live HEK293T cells. (A) Emission spectra of YNLX (ATP), with and without ATP. (B) ATP titration curve of YNLX(ATP). The bioluminescence ratio was calculated from the peaks at 490 and 530 nm. **(C)** Auto-bioluminescence imaging of YNLX (ATP). BRET ratio (pseudocolor images) of HEK293T cells expressing YNLX(Ca^{2+}) before and after the addition of an ATP inhibitor (20 μg/mL oligomycin A and 20 mM 2-deoxyglucose). Scale bars, 50 μm: ×40 magnification.

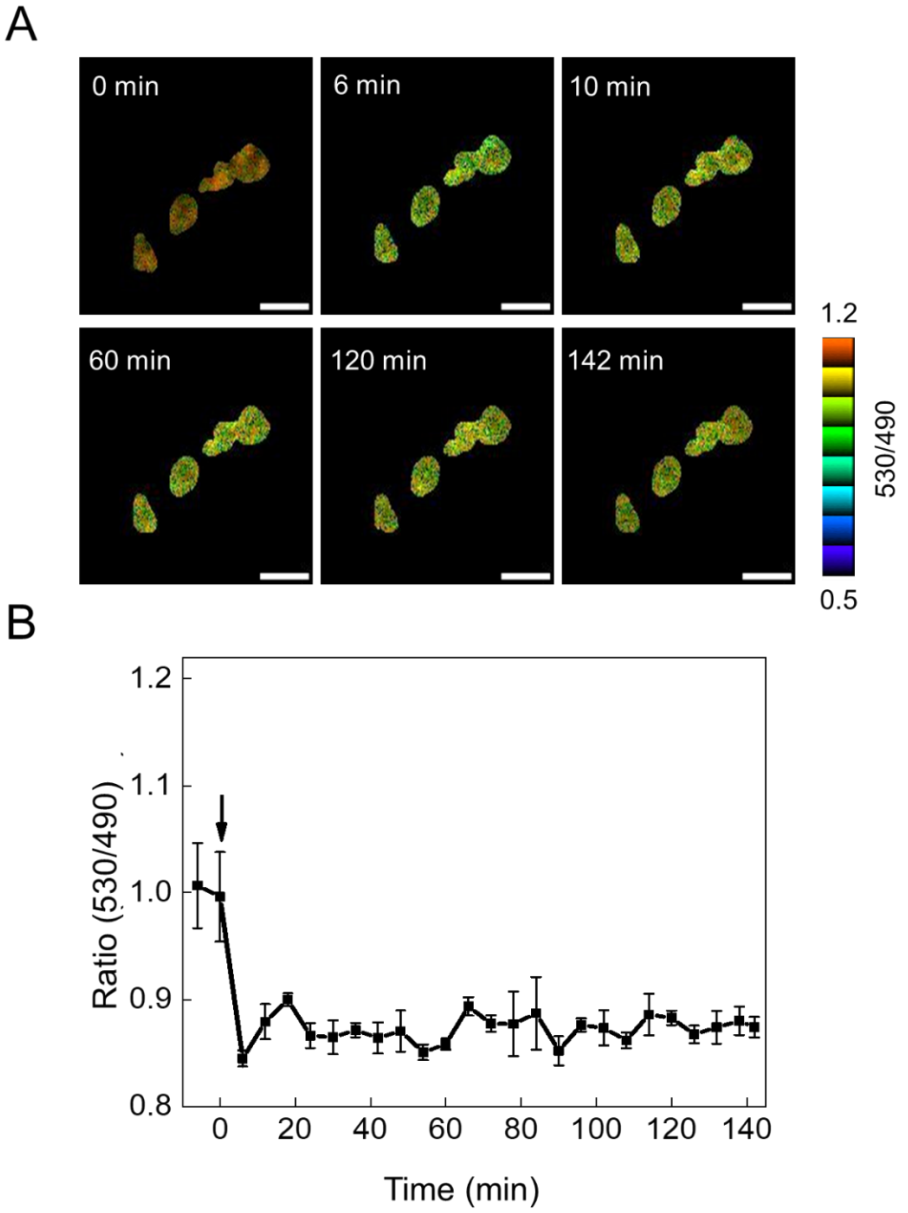

Figure 33. Time-lapse BRET imaging of cytosolic ATP levels in live HEK293T cells using YNLX (ATP). (A) Sequential images of BRET ratio in HEK293T cells expressing YNLX(ATP). ATP depletion was monitored after the addition of 20 µg/mL oligomycin A and 20 mM 2-deoxyglucose at 0 (min). Scale bars, 50 µm: ×40 magnification. **(B)** Time course of the BRET ratio in HEK293T cells expressing YNLX(ATP). The arrow indicates the time at which inhibitors were added to the medium.

Table 6. Affinity for ATP of YNLX (ATP) and other ATP sensor

	K_d (mM)	Biosensor types, donor/acceptor	References
YNLX(ATP)	2.3	Auto-LP, Lux/Venus	This study
Nano-lantern(ATP)	0.3	Non auto-LP, split-YNL	Saito, *et al*[30]
BTeam	1.7	Non auto-LP, NLuc/Venus	Yoshida, *et al*[71]
ATeam (AT1.03)	3.3	FP, mseCFP/cp173Venus	Imamura, *et al*[64]
QUEEN-2m	2.4	FP, single FP-type cpEGFP	Yaginuma, *et al*[70]

*Auto-LP (Auto-bioluminescence protein) and FP (Fluorescent protein)

3.4 Conclusion

Luciferases with non-autobioluminescent properties, such as Fluc, RLuc, and NLuc, have been used in multiplex gene assays and protein biosensors based on ratiometric strategies. However, no study has reported the use of auto-bioluminescent for multiplex gene assays and protein biosensors. In this study, I constructed a novel multiplexed gene assays and protein biosensor based on yellow NLX (YNLX) with large spectral overlap with cyan NLX (CNLX) and red NLX (RNLX). I developed a Wnt reporter using a specific Wnt promoter, 7×TCF, to generate 7×TCF-YNLX. I successfully observed long-term imaging of HEK293T cells expressing 7×TCF-YNLX. Upon the addition of agonist molecules of the Wnt protein, LiCl, bioluminescence could be detected using a microplate reader or bioluminescence microscopy. Because Wnt signalling is crucial for cell proliferation and differentiation, I examined the ability of 7×TCF-YNLX and CMV-RNLX as probes and normalizers, respectively, for high-throughput screening (HTS) applications. For transient expression, normalizer probes with different overlapping spectra are necessary because of the different transfection efficiency of each cell. As a proof-of-concept for HTS, I detected the fold-of-activation of HEK293T cells co-expressing 7×TCF-YNLX and CMV-RNLX upon the addition of different LiCl concentrations.

Furthermore, I developed novel biosensor to detect the calcium and ATP as an important ions and molecules in living cells. I successfully developed a ratiometric indicator of calcium, YNLX(Ca^{2+}), and ATP, YNLX(ATP). Both constructs showed different ratios of signals in *in vitro* and *in cellulo* experiments in the presence of the compound. YNLX(Ca^{2+}) showed an elevated 530 nm signal with the addition of Ca^{2+}, with a K_d value of 570 nM. In addition, I observed ratio changes in the luminescence images after the addition of ionomycin and $CaCl_2$. YNLX(ATP) showed a pattern similar to that of the 530 nm signal after the addition

of ATP. I detected the K_d value is 2.3 mM. I observed ATP fluctuations after the addition of an ATP inhibitor by checking the ratio signal. It should be noted that the ratiometric biosensor with auto-bioluminescent, such as Lux, is more precise and faster for detecting metabolic compounds such as ATP upon perturbation of the metabolic pathway by the metabolic inhibitor compared to relying on the intensiometric of auto-bioluminescence (auto-bioluminescence also uses ATP and NADPH to generate luciferin). In conclusion, YNLX has great potential for multipurpose applications, not only for the conventional application of a single reporter of auto-bioluminescence probes.

CHAPTER 4

CONCLUSION AND PERSPECTIVES

4.1 Conclusion

In this study, I report the development of multicolor auto-bioluminescent from bacterial luciferase (Lux) for autonomous bioluminescence imaging in live organisms. I successfully developed a novel five color variants of Lux (Nano-lanternX/NLX) by fusing it with specific fluorescent proteins (FPs). I used several FPs as an acceptor to achieve higher BRET efficiencies resulting in a shifted in the emission wavelength. To achieve higher BRET efficiency, I optimized the unistructural residues of FPs to hinder the effect of the residues on the Lux`s activity. As a result, I fused mTurquoise2, sfGFP, Venus, mKOκ, and mScarlet-I with the subunit α (LuxA) to generate cyan NLX (CNLX), green NLX (GNLX), yellow NLX (YNLX), orange NLX (ONLX), and red NLX (RNLX), respectively. In contrast, fusion of FPs with subunit β (LuxB) did not produce a higher BRET efficiency than that of LuxA. I found that CNLX shows ten-fold brightness in the purified protein compared to that of wild-type Lux. Unsurprisingly, as previously reported, BRET-based luciferase showed an enhanced quantum yield. I found that the quantum yield of NLXs was enhanced; however, there was no change in enzymatic kinetics compared to that of wild-type Lux. To test the ability of NLXs to promote auto-bioluminescence imaging in multiple organisms, I demonstrated NLXs into bacterial (*E. coli*), mammalian (HEK293T cells) and plant hosts (*N. benthamiana*). I transiently transformed them to check the specific wavelength using a commercial camera and bioluminescence microscope (EMCCD-based camera). I successfully distinguished the cells expressing CNLX, YNLX, and RNLX in bioluminescence microscope with specific optical filtering. In the plant

host, the color of the recombinant plants was successfully separated by different colors from the commercial camera and was comparable with the commons auto-bioluminescent in plants, fungal luciferase (Luz), in the luminescence intensity. Thus, my NLXs are promising bioluminescent probes because they have multicolor, no substrate is needed, and are convenient to handle and detect by the detector.

To expand the NLXs` application, I developed a novel multiplexed promoter and biosensor with a ratiometric approach based on auto-bioluminescence systems. I used 7×TCF-YNLX, as Wnt-responsive promoter, and visualized for long-term imaging upon the addition of Wnt-agonist compound, LiCl. I demonstrated dual promoters of 7×TCF-YNLX and CMV-RNLX for high-throughput screening (HTS) applications. For biosensor, I developed two types of biosensors, YNLX(Ca^{2+}) and YNLX(ATP), to detect calcium and ATP in live cells. I successfully confirmed the signal change ratio upon the addition of calcium or ATP to these biosensors and visualized them in live HEK293T cells.

In conclusion, I have reported five novel Lux variants (CNLX, GNLX, YNLX, ONLX, and RNLX) that show different emission spectral in the 475-600 nm. This development supports the development of multiple promoters and ratiometric biosensors to visualize multiple biological phenomena using autonomous bioluminescence imaging.

4.2 Perspectives

4.2.1 New versions of NLXs with brightest luminescence intensity

I have demonstrated that fusing FPs with Lux can enhance the luminescence intensity by up to ten times. However, this enhancement is necessary to achieve approximately 50- to 100-fold brighter auto-bioluminescent probes. As a result, it can be easily detected by the naked eye to observe biological responses from specific promoters or biomolecules in living organisms. Additionally, the brightest NLXs can be used for short-exposure observations, with millisecond exposure and higher spatiotemporal dynamics of calcium or voltage signaling. Therefore, a new version of the brightest Lux can be developed by further enhancing its k_{cat}. One approach is mutagenesis of the active site in LuxA.

Notably, no information on the crystal structure of *Photorhabdus luminescens* Lux has been deposited. However, a recent crystal structure obtained from *Vibrio harveyi* Lux (PDB: 3FGC) shares 85% identity with *Photorhabdus luminescens* Lux[72]. Despite this similarity, there are significant differences in the luminescence characteristics of the two species, such as the thermostability and brighter luminescence of *P. luminescens* Lux compared to that of *V. harveyi* Lux. In addition, from the recent crystal structure, there is no information on how the aldehyde substrate binds, and only the FMN substrate appears. Therefore, the molecular docking of FMN and the aldehyde substrate is necessary to determine the residue position responsible for this. In preliminary experiments, I performed molecular docking of *P. luminescens* Lux using the predicted protein structure (Alphafold2)[73]. I subsequently performed the cavity screening using CB-Dock2[74] to predict the largest cavity, which is most commonly used as the space for the active site area. Using AutoDockTools[75,76], I docked the FMN and aldehyde (tetradecanal) substrates and visualized the interaction of the substrates with the protein using LigPlot+[77]. The molecular docking of FMN of *P. luminescens* Lux

showed a similar interaction (with the addition of interaction residues on Tyr110 and Ile191) to that of FMN-bound to the crystal structure of *V. harveyi* (PDB: 3FGC) (**Figure 34)**. I also found that eight residues showed similar interactions between FMN and tetradecanal, and seven residues only interacted with tetradecanal (**Figure 35)**. In summary, I identified the residue candidates for future mutagenesis, as shown in **Table 7**. To process mutagenesis, a conventional method, such as error-prone mutagenesis, is robust in terms of time and cost, but can produce unstable proteins. Mutagenesis-based artificial intelligence (AI) is a preferable choice to increase protein activity[78–80]. Alternatively, *in vivo* mutagenesis, such as introducing specific genes into *the E. coli* EcORep strain, which can increase protein expression by up to 1000-fold for one week[81] can be applied to increase Lux activity.

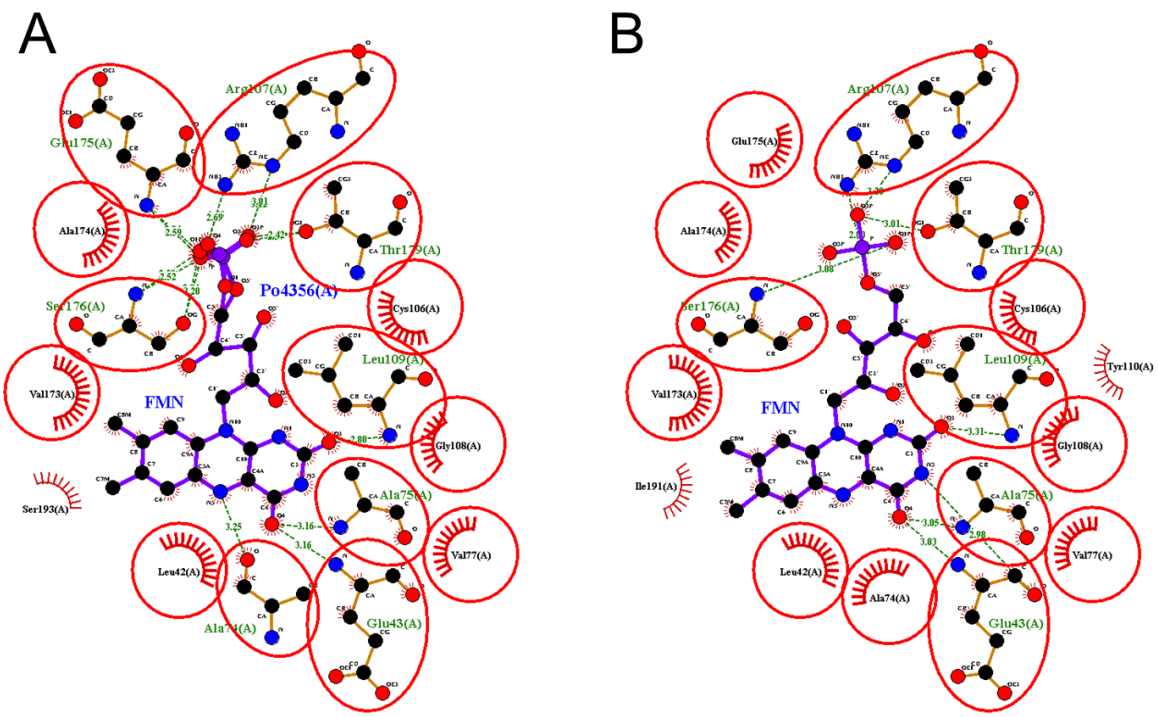

Figure 34. The responsible residues interact with FMN according to the crystal structure (PDB: 3FGC) (A) and molecular docking results (B). Red circles indicate similar interactions. Data were visualized using LigPlot+.

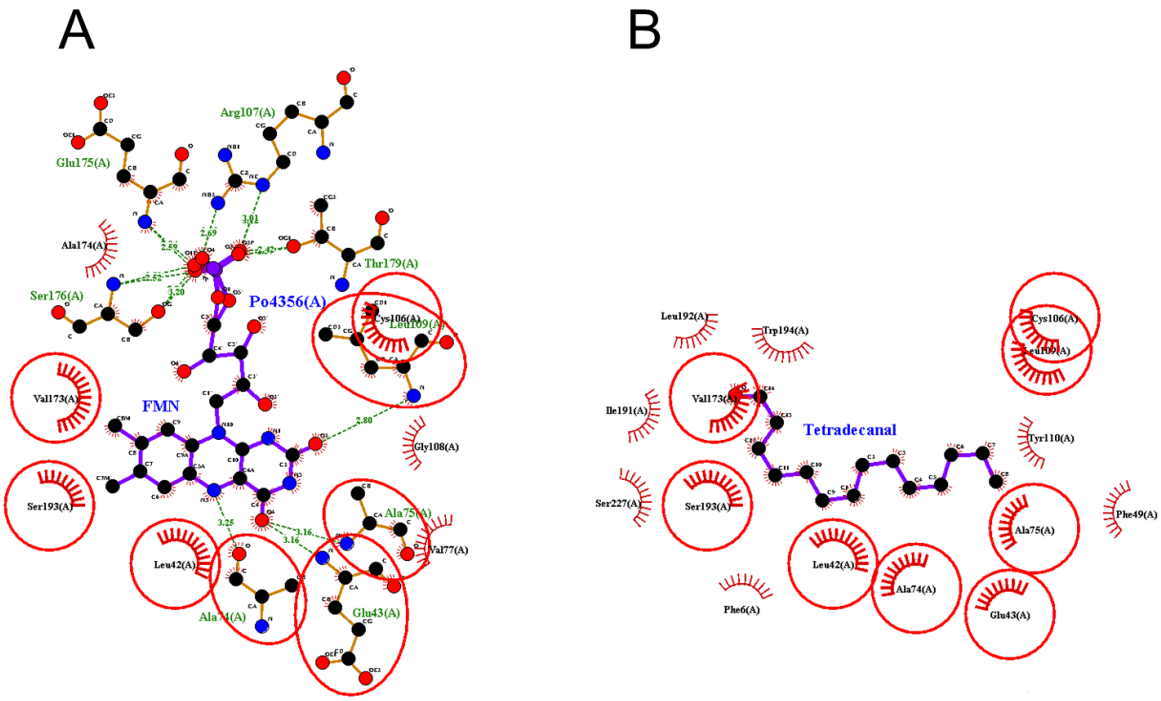

Figure 35. The responsible residues interact with FMN (A) and tetradecanal (B) based on molecular docking results. Red circles indicate similar interactions. Data were visualized using LigPlot+.

Table 7. Molecular docking results of *P. luminescencs* Lux

	Interaction	Known mutation*	Note
Cys106 (C106)	FMN and tetradecanal	C106A, C106V	Reduce activity
Glu43 (E43)	FMN and tetradecanal	-	
Leu109 (L109)	FMN and tetradecanal	-	
Ala75 (A75)	FMN and tetradecanal	A75G	Similar to wild-type
Ala74 (A74)	FMN and tetradecanal	A74F, A74G	Reduce activity
Leu42 (L42)	FMN and tetradecanal	-	-
Val173 (V173)	FMN and tetradecanal	V173A/C/F/H/I/L/N/S/T	Reduce activity
Ser193 (S193)	FMN and tetradecanal	-	-
Leu192 (L192)	Tetradecanal	-	-
Ile191 (I191)	Tetradecanal	-	-
Trp194 (W194)	Tetradecanal	-	-
Ser227 (S227)	Tetradecanal	-	-
Phe6 (F6)	Tetradecanal	F6A	Similar to wild-type
Phe49 (F49)	Tetradecanal	F49A, F49D, F49S, F49Y	Reduced activity
Tyr110 (Y110)	Tetradecanal	-	-

*Known mutation data was adopted from BRENDA database[82]

4.2.2 Development of multicolor light emitting plant in various plant hosts

Although NLXs have shown the ability to produce transient light-emitting plants, stable multicolor light-emitting plants have not yet been fully achieved. Currently, the only commercially available light-emitting plant is produced from fungal luciferase (Luz), which emits only a single color (green). However, introducing NLXs to produce multicolor light-emitting plants not only in tobacco plants but also in various other plants could prove challenging. Despite this, the light-emitting plant produced by Lux has artistic value and is more environmentally friendly since it does not produce CO_2 in its auto-bioluminescence pathways, unlike Luz.

4.2.3 Expanded of biosensor based on NLX

In this thesis, I demonstrate the ratiometric based indicator using YNLX. In addition to YNLX, other NLXs variants can also be used to develop ratiometric based indicators. In the preliminary data, I developed an orange version of the ATP sensor, which is also mimic to GO-ATeam[83] development. I modified the ONLX with insertion of ε subunit to yield mKOκ-ε subunit-LuxA, denoted as ONLX(ATP) (**Figure 36)**. In future studies, it will be possible to simultaneously visualize the dynamics of calcium and ATP with YNLX(Ca^{2+}) and ONLX(ATP) for long-term imaging in live cells.

Several genetically encoded biosensors have been developed using fluorescent proteins (FPs) as the basis, but there are only a limited number of biosensors based on bioluminescence. By using the BRET mechanism and the most recent biosensor-FP-based method, I can develop a highly effective auto-bioluminescent biosensor. In addition, inappropriate structures of the biomolecule active proteins with FPs can also affect the auto-bioluminescence intensity (**Figure 30**). Therefore, single-FP sensors, such as GCaMP[84], can also be fused with Lux to

yield new variants of biosensors based on Lux. In preliminary experiments, I developed GCaMP6f-Lux by fusing GCaMP6f[85] with the N-terminus of LuxA. I obtained the emission signal change from the purified GCaMP6f-Lux protein with and without the addition of Ca^{2+} (**Figure 37).** The mechanism of this new variant is slightly different from that of the previous YNLX(Ca^{2+}). In the absence of Ca^{2+}, the GCaMP6f protein conformation allows increased solvent access to the chromophore, leading to the protonation of the chromophore and reduced fluorescence intensity[86,87]. Consequently, it exhibited the lowest BRET efficiency. In contrast, in the presence of Ca^{2+}, the CaM and M13 conformations of GCaMP6f blocked solvent access to the chromophore, rapidly deprotonated, and increased the fluorescence intensity[86,87]. The BRET efficiency of Lux showed the highest efficiency and shifted the emission wavelength (**Figure 37)**. In that case, the BRET did not occur by the distance as YNLX(Ca^{2+}), but by the fluorescence change of the GCaMP6f protein conformation.

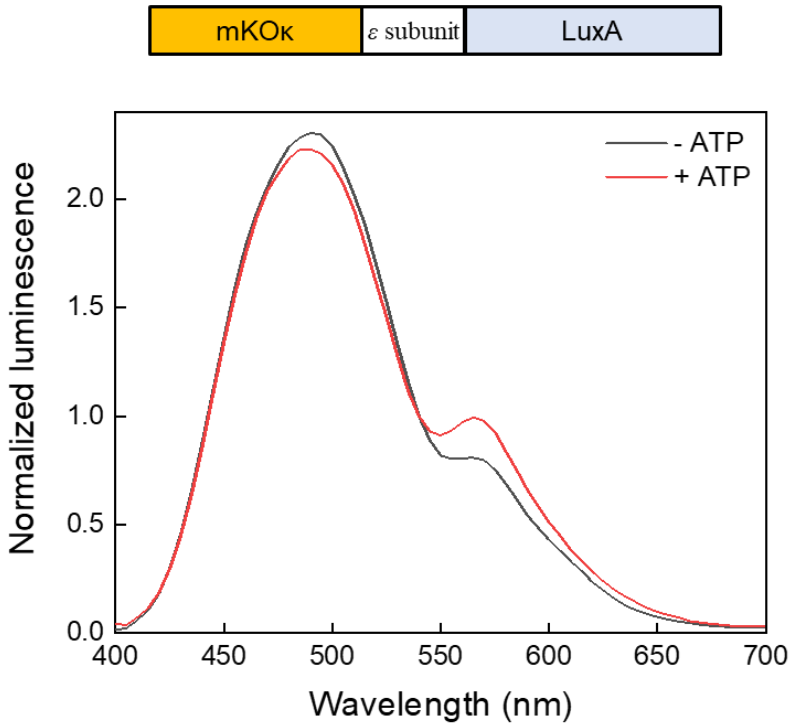

Figure 36. The emission spectra of ONLX(ATP) with and without ATP.

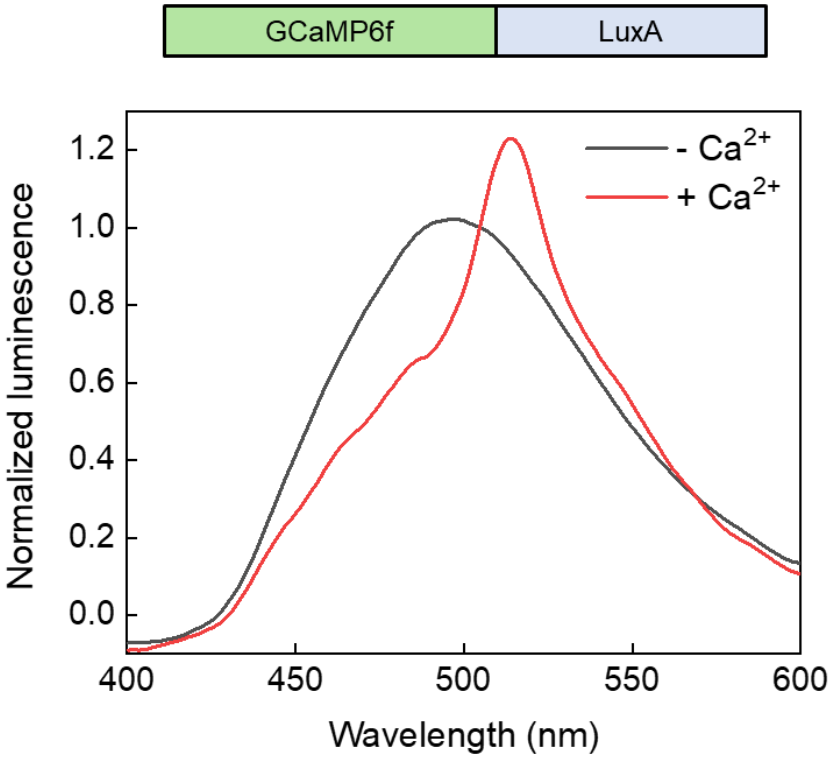

Figure 36. The emission spectra of GCaMP6f-Lux with and without ATP

REFERENCES

1. Shimomura, O. *Bioluminescence: Chemical Principles and Methods (3rd Edition)* (WORLD SCIENTIFIC, 2012).
2. Kricka, L. J. & Leach, F. R. Firefly luciferase: mechanism of action, cloning and expression of the active enzyme. *J. Biolumin. Chemilumin.* **3**, (1989).
3. Hall, M. P. *et al.* Engineered luciferase reporter from a deep sea shrimp utilizing a novel imidazopyrazinone substrate. *ACS Chem. Biol.* **7**, (2012).
4. England, C. G., Ehlerding, E. B. & Cai, W. NanoLuc: A small luciferase is brightening up the field of bioluminescence. *Bioconjug. Chem.* **27**, 1175–1187 (2016).
5. Meighen, E. A. Molecular biology of bacterial bioluminescence. *Microbiol Rev* **55**, 123–142 (1991).
6. Purtov, K. V. *et al.* The chemical basis of fungal bioluminescence. *Angewandte Chemie - International Edition* **54**, (2015).
7. Kotlobay, A. A. *et al.* Genetically encodable bioluminescent system from fungi. *Proc. Natl. Acad. Sci. U. S. A.* **115**, 12728–12732 (2018).
8. Ahn, J. M. *et al.* Prediction and classification of the modes of genotoxic actions using bacterial biosensors specific for DNA damages. *Biosens. Bioelectron.* **25**, (2009).
9. Kotova, V. Y., Manukhov, I. V. & Zavilgelskii, G. B. Lux-biosensors for detection of SOS-response, heat shock, and oxidative stress. *Appl. Biochem. Microbiol.* **46**, (2010).
10. Mitchell, R. J. & Gu, M. B. Construction and evaluation of nagR-nagAa::lux fusion strains in biosensing for salicylic acid derivatives. *Appl. Biochem. Biotechnol.* **120**, (2005).
11. Xu, T., Gilliam, M., Sayler, G., Ripp, S. & Close, D. Screening for androgen agonists using autonomously bioluminescent HEK293 reporter cells. *Biotechniques* **71**, (2021).
12. Kaskova, Z. M. *et al.* Mechanism and color modulation of fungal bioluminescence. *Sci. Adv.* **3**, (2017).
13. Mitiouchkina, T. *et al.* Plants with genetically encoded autoluminescence. *Nat. Biotechnol.* **38**, (2020).
14. Khakhar, A. *et al.* Building customizable auto-luminescent luciferase-based reporters in plants. *eLife* **9**, (2020).

15. Delong, E. F., Steinhauer, D., Israel, A. & Nealson, K. H. Isolation of the lux genes from *Photobacterium leiognathi* and expression in *Escherichia coli*. *Gene* **54**, (1987).
16. Szittner, R. & Meighen, E. Nucleotide sequence, expression, and properties of luciferase coded by lux genes from a terrestrial bacterium. *J. Biol. Chem.* **265**, (1990).
17. Gunsalus-Miguel, A., Meighen, E. A., Nicoli, M. Z., Nealson, K. H. & Hastings, J. W. Purification and properties of bacterial luciferases. *J. Biol. Chem.* **247**, (1972).
18. Brodl, E., Winkler, A. & Macheroux, P. Molecular Mechanisms of Bacterial Bioluminescence. *Comput. Struct. Biotechnol. J.* **16**, 551–564 (2018).
19. Campbell, Z. T., Weichsel, A., Montfort, W. R. & Baldwin, T. O. Crystal structure of the bacterial luciferase/flavin complex provides insight into the function of the β subunit. *Biochemistry* **48**, 6085–6094 (2009).
20. Fisher, A. J., Thompson, T. B., Thoden, J. B., Baldwin, T. O. & Rayment, I. The 1.5-Å resolution crystal structure of bacterial luciferase in low salt conditions. *J. Biol. Chem.* **271**, (1996).
21. Ruby, E. G. & Nealson, K. H. A luminous bacterium that emits yellow light. *Science* **4288**, (1977).
22. Macheroux, P. *et al.* Purification of the yellow fluorescent protein from *Vibrio fischeri* and identity of the flavin chromophore. *Biochem. Biophys. Res. Commun.* **146**, (1987).
23. Small, E. D., Koka, P. & Lee, J. Lumazine protein from the bioluminescent bacterium *Photobacterium phosphoreum*, purification and characterization. *J. Biol. Chem.* **255**, (1980).
24. Titushin, M. S., Feng, Y., Lee, J., Vysotski, E. S. & Liu, Z. J. Protein-protein complexation in bioluminescence. *Protein and Cell* (2011).
25. Lee, J., O'Kane, D. J. & Visser, A. J. W. G. Spectral properties and function of two lumazine proteins from Photobacterium. *Biochemistry* **24**, (1985).
26. Jares-Erijman, E. A. & Jovin, T. M. FRET imaging. *Nat. Biotechnol.* **21**, (2003).
27. Berney, C. & Danuser, G. FRET or no FRET: A quantitative comparison. *Biophys. J.* **84**, (2003).
28. Angers, S. *et al.* Detection of β 2 -adrenergic receptor dimerization in living cells using bioluminescence resonance energy transfer (BRET) . *Proc. Natl. Acad. Sci. U. S. A.* **97**, (2000).

29. Xu, Y., Piston, D. W. & Johnson, C. H. A bioluminescence resonance energy transfer (BRET) system: Application to interacting circadian clock proteins. *Proc. Natl. Acad. Sci. U. S. A.* **96**, (1999).
30. Saito, K. *et al.* Luminescent proteins for high-speed single-cell and whole-body imaging. *Nat. Commun.* **3**, 1262 (2012).
31. Takai, A. *et al.* Expanded palette of Nano-lanterns for real-time multicolor luminescence imaging. *Proc. Natl. Acad. Sci. U. S. A.* **112**, 4352–4356 (2015).
32. Suzuki, K. *et al.* Five colour variants of bright luminescent protein for real-time multicolour bioimaging. *Nat. Commun.* **7**, 13718 (2016).
33. Zhao, H. *et al.* Characterization of coelenterazine analogs for measurements of Renilla luciferase activity in live cells and living animals. *Mol. Imaging.* **3**, 43–54 (2004).
34. Gregor, C., Gwosch, K. C., Sahl, S. J. & Hell, S. W. Strongly enhanced bacterial bioluminescence with the ilux operon for single-cell imaging. *Proc. Natl. Acad. Sci. U. S. A.* **115**, (2018).
35. Gregor, C. *et al.* Autonomous bioluminescence imaging of single mammalian cells with the bacterial bioluminescence system. *Proc. Natl. Acad. Sci. U. S. A.* **116**, 26491–26496 (2019).
36. Lin, L. Y.-C., Szittner, R., Friedman, R. & Meighen, E. A. Changes in the kinetics and emission spectrum on mutation of the chromophore-binding platform in *Vibrio harveyi* Luciferase. *Biochemistry* **43**, 3183–3194 (2004).
37. Daubner, S. C., Astorga, A. M., Leisman, G. B. & Baldwin, T. O. Yellow light emission of *Vibrio fischeri* strain Y-1: purification and characterization of the energy-accepting yellow fluorescent protein. *Proc. Natl. Acad. Sci. U. S. A.* **84**, 8912–8916 (1987).
38. Petushkov, V. N., Gibson, B. G. & Lee, J. Direct measurement of excitation transfer in the protein complex of bacterial luciferase hydroxyflavin and the associated yellow fluorescence proteins from *Vibrio fischeri* Y1. *Biochemistry* **35**, 8413–8418 (1996).
39. Sato, Y. *et al.* Crystal structures of the lumazine protein from *Photobacterium kishitanii* in complexes with the authentic chromophore, 6,7-Dimethyl- 8-(1′-Ribityl) Lumazine, and its analogues, riboflavin and flavin mononucleotide, at high resolution. *J. Bacteriol.* **192**, 127–133 (2010).
40. Xia, Y. *et al.* T5 exonuclease-dependent assembly offers a low-cost method for efficient cloning and site-directed mutagenesis. *Nucleic Acids Res.* **47**, e15–e15 (2019).

41. Phonbuppha, J. *et al.* A Minimized chemoenzymatic cascade for bacterial luciferase in bioreporter applications. *ChemBioChem* **21**, 2073–2079 (2020).
42. Ando, Y. *et al.* Development of a quantitative bio/chemiluminescence spectrometer determining quantum yields: re-examination of the aqueous luminol chemiluminescence standard. *Photochem. Photobiol.* **83**, 1205–1210 (2007).
43. Mirdita, M. *et al.* ColabFold: making protein folding accessible to all. *Nat. Methods* **19**, (2022).
44. Pettersen, E. F. *et al.* UCSF Chimera - A visualization system for exploratory research and analysis. *J. Comput. Chem.* **25**, (2004).
45. Nagai, T. *et al.* A variant of yellow fluorescent protein with fast and efficient maturation for cell-biological applications. *Nat. Biotechnol.* **20**, 87–90 (2002).
46. Kaku, T., Sugiura, K., Entani, T., Osabe, K. & Nagai, T. Enhanced brightness of bacterial luciferase by bioluminescence resonance energy transfer. *Sci. Rep.* **11**, 14994 (2021).
47. Goedhart, J. *et al.* Structure-guided evolution of cyan fluorescent proteins towards a quantum yield of 93%. *Nat. Commun.* **3**, 751 (2012).
48. Pédelacq, J.-D., Cabantous, S., Tran, T., Terwilliger, T. C. & Waldo, G. S. Engineering and characterization of a superfolder green fluorescent protein. *Nat. Biotechnol.* **24**, 79–88 (2006).
49. Tsutsui, H., Karasawa, S., Okamura, Y. & Miyawaki, A. Improving membrane voltage measurements using FRET with new fluorescent proteins. *Nat. Methods.* **5**, 683–685 (2008).
50. Bindels, D. S. *et al.* mScarlet: a bright monomeric red fluorescent protein for cellular imaging. *Nat. Methods* **14**, 53–56 (2017).
51. Chu, J. *et al.* A bright cyan-excitable orange fluorescent protein facilitates dual-emission microscopy and enhances bioluminescence imaging in vivo. *Nat. Biotechnol.* **34**, 760–767 (2016).
52. Mukherjee, S., Manna, P., Douglas, N., Chapagain, P. P. & Jimenez, R. Conformational dynamics of mCherry variants: a link between side-chain motions and fluorescence brightness. *J. Phys. Chem. B.* **127**, 52–61 (2023).
53. Dunn, A. K., Rader, B. A., Stabb, E. V. & Mandel, M. J. Regulation of bioluminescence in *Photobacterium leiognathi* strain KNH6. *J. Bacteriol.* **197**, (2015).

54. Gammon, S. T., Leevy, W. M., Gross, S., Gokel, G. W. & Piwnica-Worms, D. Spectral unmixing of multicolored bioluminescence emitted from heterogeneous biological sources. *Anal. Chem.* **78**, 1520–1527 (2006).
55. Jawanda, N., Ahmed, K. & Tu, S.-C. *Vibrio harveyi* flavin reductase−luciferase fusion protein mimics a single-component bifunctional monooxygenase. *Biochemistry* **47**, 368–377 (2008).
56. Wang, Y. *et al.* Optimization of a 2A self-cleaving peptide-based multigene expression system for efficient expression of upstream and downstream genes in silkworm. *Mol. Genet. Genomics* **294**, 849–859 (2019).
57. Krichevsky, A., Meyers, B., Vainstein, A., Maliga, P. & Citovsky, V. Autoluminescent plants. *PLoS One* **5**, (2010).
58. Niehrs, C. The complex world of WNT receptor signalling. *Nat. Rev. Mol. Cell Biol.* **13,** (2012).
59. Liu, J. *et al.* Wnt/β-catenin signalling: function, biological mechanisms, and therapeutic opportunities. *Sig. Transduct. Target Ther.* **7**, (2022).
60. Cruciat, C. M. & Niehrs, C. Secreted and transmembrane Wnt inhibitors and activators. *Cold Spring Harb. Perspect. Biol.* **5**, (2013).
61. Kaihara, A., Umezawa, Y. & Furukawa, T. Bioluminescent indicators for Ca^{2+} based on split Renilla luciferase complementation in living cells. *Anal. Sci.* **24**, (2008).
62. Saito, K. *et al.* Auto-luminescent genetically-encoded ratiometric indicator for real-time Ca^{2+} imaging at the single cell level. *PLoS One* **5**, (2010).
63. Thestrup, T. *et al.* Optimized ratiometric calcium sensors for functional in vivo imaging of neurons and T lymphocytes. *Nat. Methods* **11**, 175–182 (2014).
64. Imamura, H. *et al.* Visualization of ATP levels inside single living cells with fluorescence resonance energy transfer-based genetically encoded indicators. *Proc. Natl. Acad. Sci. U. S. A.* **106**, 15651–15656 (2009).
65. Schneider, C. A., Rasband, W. S. & Eliceiri, K. W. NIH Image to ImageJ: 25 years of image analysis. *Nat. Methods* **9**, 671–675 (2012).
66. Takai, A. *et al.* Anterior neural development requires Del1, a matrix-associated protein that attenuates canonical Wnt signaling via the Ror2 pathway. *Development* **137**, 3293–3302 (2010).

67. Phonbuppha, J., Tinikul, R., Ohmiya, Y. & Chaiyen, P. High sensitivity and low-cost flavin luciferase (FLUXVc)-based reporter gene for mammalian cell expression. *J. Biol. Chem.* **299**, 104639 (2023).
68. Nagai, T., Yamada, S., Tominaga, T., Ichikawa, M. & Miyawaki, A. Expanded dynamic range of fluorescent indicators for Ca^{2+} by circularly permuted yellow fluorescent proteins. *Proc. Natl. Acad. Sci. U. S. A.* **101**, 10554–10559 (2004).
69. Yang, J. *et al.* Coupling optogenetic stimulation with NanoLuc-based luminescence (BRET) Ca^{2+} sensing. *Nat. Commun.* **7**, (2016).
70. Yaginuma, H. *et al.* Diversity in ATP concentrations in a single bacterial cell population revealed by quantitative single-cell imaging. *Sci. Rep.* **4**, (2014).
71. Yoshida, T., Kakizuka, A. & Imamura, H. BTeam, a novel BRET-based biosensor for the accurate quantification of ATP concentration within living cells. *Sci. Rep.* **6**, (2016).
72. Urbanczyk, H., Ast, J. C., Kaeding, A. J., Oliver, J. D. & Dunlap, P. V. Phylogenetic analysis of the incidence of lux gene horizontal transfer in Vibrionaceae. *J. Bacteriol.* **190**, (2008).
73. Jumper, J. *et al.* Highly accurate protein structure prediction with AlphaFold. *Nature* **596**, (2021).
74. Liu, Y. *et al.* CB-Dock2: improved protein-ligand blind docking by integrating cavity detection, docking and homologous template fitting. *Nucleic Acids Res.* **50**, (2022).
75. Forli, S. *et al.* Computational protein-ligand docking and virtual drug screening with the AutoDock suite. *Nat. Protoc.* **11**, (2016).
76. Eberhardt, J., Santos-Martins, D., Tillack, A. F. & Forli, S. AutoDock Vina 1.2.0: New docking methods, expanded force field, and python bindings. *J. Chem. Inf. Model* **61**, (2021).
77. Laskowski, R. A. & Swindells, M. B. LigPlot+: Multiple ligand-protein interaction diagrams for drug discovery. *J. Chem. Inf. Model* **51**, (2011).
78. Hu, R. *et al.* Protein engineering via Bayesian optimization-guided evolutionary algorithm and robotic experiments. *Brief Bioinform.* **24**, (2023).
79. Shroff, R. *et al.* Discovery of novel gain-of-function mutations guided by structure-based deep learning. *ACS Synth. Biol.* **9**, (2020).
80. Saito, Y. *et al.* Machine-Learning-Guided mutagenesis for directed evolution of fluorescent proteins. *ACS Synth. Biol.* **7**, (2018).

81. Tian, R. *et al.* Establishing a synthetic orthogonal replication system enables accelerated evolution in E. coli. *Science* **383**, (2024).
82. Chang, A. *et al.* BRENDA, the ELIXIR core data resource in 2021: New developments and updates. *Nucleic Acids Res.* **49**, (2021).
83. Nakano, M., Imamura, H., Nagai, T. & Noji, H. Ca^{2+} regulation of mitochondrial ATP synthesis visualized at the single cell level. *ACS Chem. Biol.* **6**, (2011).
84. Nakai, J., Ohkura, M. & Imoto, K. A high signal-to-noise Ca^{2+} probe composed of a single green fluorescent protein. *Nat. Biotechnol.* **19**, (2001).
85. Dana, H. *et al.* High-performance calcium sensors for imaging activity in neuronal populations and microcompartments. *Nat. Methods* **16**, (2019).
86. Akerboom, J. *et al.* Crystal structures of the GCaMP calcium sensor reveal the mechanism of fluorescence signal change and aid rational design. *J. Biol. Chem* **284**, (2009).
87. Barnett, L. M., Hughes, T. E. & Drobizhev, M. Deciphering the molecular mechanism responsible for GCaMP6m's Ca^{2+} dependent change in fluorescence. *PLoS One* **12**, (2017).

ACKNOWLEDGEMENTS

I am gracious to everyone who has supported me during my doctoral journey. To begin, I extend my heartfelt thanks to my supervisor Prof. Takeharu Nagai. Without his guidance, generous support, unwavering patience, kindness, and enthusiastic encouragement, this thesis would not have been possible. My gratitude knows no bounds.

I would like to express my sincere gratitude to my sub-supervisor, Asst. Prof. Mitsuru Hattori for his exceptional kindness and help during the development of this research. His valuable and constructive suggestions were instrumental to the successful completion of this thesis.

I am grateful to express my appreciation to my thesis committee: Prof. Takeshi Yagi (Graduate school of Frontier Biosciences (FBS), Osaka University), Prof. Masahiro Ueda (FBS, Osaka University), and Prof. Tatsuro Fukagawa (FBS, Osaka University), for their valuable feedback that has broadened my comprehension and enriched my knowledge.

I am grateful to my previous professors in the Nagai Lab, particularly Asst. Prof. Kenji Osabe and Assoc. Prof. Tomoki Matsuda for their invaluable guidance and encouragement. I extend my sincere appreciation to all the lab members for their unwavering support and assistance. For all thanks to the secretaries for helping me with the document-related work. I also thank the Japan Government and the Ministry of Education, Culture, Sports, Science, and Technology (MEXT) for financial support by MEXT scholarship.

Finally, I would like to dedicate all of my hard work, particularly this thesis, to my loved ones, especially my daughter, Syafira Hannah, and my wonderful wife, Sarah, who provided me with invaluable support during my research. .

LIST OF ACADEMIC ACCOMPLISHMENTS

Publication

1. **Kusuma, SH.,** Hattori M., and Nagai T., Autonomous multicolor bioluminescence imaging in bacteria, mammalian, and plant hosts. *bioRxiv.* doi: https://doi.org/10.1101/2024.04.28.591567 (2024).

Conferences

1. **Kusuma, SH.,** *2023 年度生理研研究会*, September 14th–15th 2023, Japan

2. **Kusuma, SH.,** Hattori M., and Nagai T., Multicolor Autoluminescent Reporters based on Bacterial Bioluminescence System, *The 61st Annual Meeting of the Biophysical Society of Japan*, November 14th–16th 2023, Japan

3. **Kusuma, SH.,** Hattori M., and Nagai T., Multicolor Autoluminescent Reporters based on Bacterial Bioluminescent System, *第 1 回関西生物物理学研究会*, March 18th–19th 2024, Japan

4. **Kusuma, SH.,** Hattori M., and Nagai T., Multicolor autonomous bioluminescence imaging based on bacterial bioluminescence system, *21st International Union for Pure and Applied Biophysics and 62nd Biophysics Society of Japan*, June 24th–28th 2024, Japan